The Plant Cell, Vol. 32: 2878–2897, September 2020, www.plantcell.org © 2020 ASPB.

Check for updates

Casein Kinase 1 Regulates Cytorhabdovirus Replication and Transcription by Phosphorylating a Phosphoprotein Serine-Rich Motif

Qiang Gao,[a,1] Teng Yan,[a,1] Zhen-Jia Zhang,[a,1] Song-Yu Liu,[a] Xiao-Dong Fang,[a] Dong-Min Gao,[a] Yi-Zhou Yang,[a] Wen-Ya Xu,[a] Ji-Hui Qiao,[a] Qing Cao,[a] Zhi-Hang Ding,[a] Ying Wang,[b] Jialin Yu,[a] and Xian-Bing Wang[a,2]

[a] State Key Laboratory of Agro-Biotechnology, College of Biological Sciences, China Agricultural University, Beijing 100193, China
[b] College of Plant Protection, China Agricultural University, Beijing 100193, China

Casein kinase 1 (CK1) family members are conserved Ser/Thr protein kinases that regulate important developmental processes in all eukaryotic organisms. However, the functions of CK1 in plant immunity remain largely unknown. *Barley yellow striate mosaic virus* (BYSMV), a plant cytorhabdovirus, infects cereal crops and is obligately transmitted by the small brown planthopper (SBPH; *Laodelphax striatellus*). The BYSMV phosphoprotein (P) exists as two forms with different mobilities corresponding to 42 kD (P42) and 44 kD (P44) in SDS-PAGE gels. Mass spectrometric analyses revealed a highly phosphorylated serine-rich (SR) motif at the C-terminal intrinsically disordered region of the P protein. The Ala-substitution mutant (P^{S5A}) in the SR motif stimulated virus replication, whereas the phosphorylation-mimic mutant (P^{S5D}) facilitated virus transcription. Furthermore, P^{S5A} and P^{S5D} associated preferentially with nucleocapsid protein–RNA templates and the large polymerase protein to provide optimal replication and transcription complexes, respectively. Biochemistry assays demonstrated that plant and insect CK1 protein kinases could phosphorylate the SR motif and induce conformational changes from P42 to P44. Moreover, overexpression of CK1 or a dominant-negative mutant impaired the balance between P42 and P44, thereby compromising virus infections. Our results demonstrate that BYSMV recruits the conserved CK1 kinases to achieve its cross-kingdom infection in host plants and insect vectors.

INTRODUCTION

Phosphorylation is one of the most important posttranslational modifications in eukaryotic cells and has important roles in enzyme activation, transcription, and biotic/abiotic stress responses (Friso and van Wijk, 2015; Millar et al., 2019). As a reversible process, phosphorylation is catalyzed by protein kinases, while dephosphorylation is achieved by protein phosphatases (Friso and van Wijk, 2015; Millar et al., 2019). Casein kinase 1 (CK1) proteins are highly conserved Ser/Thr protein kinases in eukaryotes. CK1-type kinases have been extensively studied in their regulatory role of divergent biological processes in yeast and animals (Gross and Anderson, 1998; Knippschild et al., 2005). By contrast, only a few studies have focused on the biological roles of plant CK1 proteins. Arabidopsis (*Arabidopsis thaliana*) CK1.3 and CK1.4 phosphorylate the photoreceptor cryptochrome 2 to regulate blue light signaling (Tan et al., 2013). Arabidopsis CK1.8 regulates ethylene biosynthesis by phosphorylating ACC SYNTHASE5 (ACS5), a key enzyme in ethylene biosynthesis, thereby promoting ACS5 turnover (Tan and Xue, 2014). Arabidopsis CASEIN KINASE 1-LIKE6 (CKL6) mainly plays a role in macromolecular trafficking at plasmodesmata sites (Lee et al., 2005). A rice (*Oryza sativa*) CK1 has been shown to be involved in signal transduction and hormone metabolism (Liu et al., 2003). However, the function of CK1 in plant immunity has not yet been elucidated.

The virus family *Rhabdoviridae* contains bacilliform or bullet-shaped, enveloped viruses that have monopartite single-stranded, negative-sense RNA genomes (Ammar et al., 2009). More than 160 rhabdoviruses infect a broad range of hosts from human, wildlife, livestock, to plant. Plant rhabdoviruses infect various monocot and dicot plants, including agriculturally significant crops such as wheat (*Triticum aestivum*), rice, barley (*Hordeum vulgare*), maize (*Zea mays*), potato (*Solanum tuberosum*), and tomato (*Solanum lycopersicum*). Plant rhabdoviruses are taxonomically divided into six genera: *Cytorhabdovirus*, *Dichorhavirus*, *Varicosavirus*, *Alphanucleorhabdovirus*, *Betanucleorhabdovirus*, and *Gammanucleorhabdovirus* (Dietzgen et al., 2020). Previous work on plant rhabdoviruses has largely focused on biochemical and molecular analyses of viral proteins during ectopic expression in plant cells, but not in the context of authentic virus infections due to the lack of available reverse genetic systems. Recently, Wang and colleagues developed the first reverse genetics system of plant negative-stranded RNA viruses in *Nicotiana benthamiana* plants, which facilitates investigation of the biological functions of viral proteins (Jackson et al., 2005; Wang et al., 2015; Jackson and Li, 2016).

A typical rhabdovirus genome encodes five conserved structural proteins: the nucleocapsid protein (N), a phosphoprotein (P), a matrix protein (M), a glycoprotein (G), and the large subunit (L) of the RNA-dependent RNA polymerase complex (RdRp). These genes are organized in the conserved order $3'-N-P-M-G-L-5'$ (Jackson et al., 2005; Mann and Dietzgen, 2014). In addition, plant rhabdoviruses encode one or more ancillary proteins in the $N-P$, $P-M$, or $G-L$ gene junctions (Walker et al.,

[1] These authors contributed equally to this work.
[2] Address correspondence to wangxianbing@cau.edu.cn.
The author responsible for distribution of materials integral to the findings presented in this article in accordance with the policy described in the Instructions for Authors (www.plantcell.org) is: Xian-Bing Wang (wangxianbing@cau.edu.cn).
www.plantcell.org/cgi/doi/10.1105/tpc.20.00369

IN A NUTSHELL

Background: Phosphorylation is a widespread post-translational modification of cellular proteins in eukaryotic cells. For instance, Casein kinase 1 (CK1) enzymes are highly conserved Ser/Thr protein kinases that regulate critical aspects of development in yeast, plants, and animals. Accumulating evidence suggests that many host protein kinases play pivotal roles when plants are infected by a virus by phosphorylating viral proteins. Rhabdoviruses are a group of viruses with negative-sense single-stranded RNA genomes that cause significant losses to agriculture production worldwide when they infect crops. Most plant rhabdoviruses are obligately transmitted by arthropod vectors in a persistent propagative manner. Recent breakthroughs in reverse genetics systems applied to plant rhabdoviruses now allow an investigation of virus-insect-plant interactions.

Question: We wanted to know whether a conserved protein kinase might be implicated in the cross-kingdom infections of host plants and insect vectors by plant rhabdoviruses. How does protein kinases regulate infections of plant rhabdoviruses?

Findings: We found that the phosphoprotein (P) of *barley yellow striate mosaic virus* (BYSMV), a plant cytorhabdovirus, was phosphorylated by plant and insect CK1 protein kinases. Mass spectrometry analysis revealed that CK1 phosphorylated a Ser-rich (SR) motif at the C terminal intrinsically disordered region of BYSMV P. Phosphorylation of BYSMV P results in the production of two P forms with different mobilities corresponding to 42 kDa (P42) and 44 kDa (P44) in protein gels. Using a reverse genetics system in BYSMV, we found that BYSMV P42 and P44 stimulated viral replication and transcription, respectively. Overexpression of CK1, or a dominant-negative CK1 mutant, impaired the balance between P42 and P44, thereby compromising viral infection. Our results revealed that BYSMV recruits conserved CK1 kinases for cross-kingdom infections in host plants and insect vectors.

Next steps: We wish to determine the spatial and temporal expression of the different phosphorylation forms of BYSMV P, as well as their functions during BYSMV infections in host plants and insect vectors. Whether CK1 protein kinases are common modulators of other plant and animal rhabdoviruses also remains an open question for investigation.

2011). The rhabdovirus nucleocapsid is a minimal infectious unit that comprises the genomic RNA (gRNA) associated with the N, P, and L core proteins. During replication, the nascent rhabdovirus gRNAs and antigenomic RNAs (agRNAs) are rapidly encapsidated by the N proteins to form a long helical N–gRNA complex that serves as a template for RdRp-mediated transcription and genome replication (Moyer et al., 1991). The rhabdovirus P protein provides a noncatalytic cofactor that facilitates access of the L protein to N–RNA template. In addition, the P protein forms N^0-P complexes with nascent RNA-free N (N^0) proteins to solubilize N^0 and to encapsulate gRNAs and agRNAs generated during replication (Emerson and Schubert, 1987; Moyer et al., 1991; Green and Luo, 2009; Rahmeh et al., 2012). Rhabdovirus transcription and replication are regulated in a dynamic balance by the polymerase complex, and an intriguing open question is how the viral RdRp fine-tunes the balance between transcription and replication.

Barley yellow striate mosaic virus (BYSMV) is a member of the genus *Cytorhabdovirus* and elicits chlorotic striations and mosaic symptoms in cereal plant species. BYSMV is transmitted in a persistent-propagative manner by the small brown planthopper (SBPH; *Laodelphax striatellus*; Cao et al., 2018). The BYSMV genome consists of 12,706 nucleotides and encodes five conserved structural proteins and five ancillary proteins in the order $3'-N-P-P3-P4/P5-P6-M-G-P9-L-5'$ (Yan et al., 2015). We recently developed a BYSMV antigenomic minireplicon (BYSMV-agMR) system in *N. benthamiana* leaves (Fang et al., 2019). We subsequently rescued BYSMV (i.e., reconstituted a functional and infectious genome) from full-length cDNA clones and developed BYSMV vectors as versatile delivery platforms in monocot plants and planthoppers (Gao et al., 2019). Using these genetic systems, we recently demonstrated that the BYSMV P protein hijacks the host deadenylation factor CARBON CATABOLITE REPRESSION4 (CCR4) to promote viral replication (Zhang et al., 2020). Here, we explored the regulation of BYSMV P phosphorylation in viral transcription and replication.

Accumulating evidence suggests that many host protein kinases play pivotal roles in viral life cycles by phosphorylating both viral and host cellular proteins (Jakubiec and Jupin, 2007; Hu et al., 2015; Wang, 2015; Zhao et al., 2015; Hoover and Kao, 2016; Zhong et al., 2017; Mei et al., 2018). However, the role of phosphorylation during plant negative-stranded RNA virus infections has not been described. Here, we first undertook mass spectrometric analyses of BYSMV P proteins to identify physiologically relevant phosphorylation sites. Intriguingly, we identified a highly phosphorylated serine-rich (SR) motif at the C-terminal domain intrinsically disordered region (IDR_{CTD}) of BYSMV P. We then used reverse genetic approaches to investigate the effects of these phosphorylation events on BYSMV infections. We present several lines of evidence showing that the SR motif of BYSMV P is phosphorylated by the conserved CK1 family of plant and insect hosts to finely regulate the balance of BYSMV transcription and replication.

RESULTS

Identification of BYSMV P Phosphorylated Residues by Mass Spectrometry

To investigate the phosphorylated forms of BYSMV P in vivo, we performed immunoblot analyses to detect BYSMV P proteins

isolated from *N. benthamiana* leaves infiltrated with the BYSMV agMR (Fang et al., 2019) via Agrobacterium (*Agrobacterium tumefasciens*), from BYSMV-infected SBPHs, and from barley plants infiltrated with BYSMV agMR, using purified BYSMV virions from infected barley plants as a positive control. We detected two main bands for BYSMV P in SDS-PAGE gels with slightly different mobilities, corresponding to 42 kD (designated P42) and 44 kD (designated P44; Figure 1A). Notably, P44 was the principal form in BYSMV virions (Figure 1A, lane 7). In BYSMV-agMR assays, BYSMV P mainly existed as the P42 form 2 d postinfiltration (2 dpi; Figure 1B). Subsequently, the appearance of P44 was accompanied by red fluorescent protein (RFP) accumulation and agMR replication at 4 and 6 dpi (Figure 1B). The RFP coding sequence was inserted in between the virus *N* and *P* genes in the infectious clone and provides a positive control for transcription of the viral genome. The P44:P42 ratio gradually increased during BYSMV infections in barley plants (Figure 1C). Collectively, these results suggest that P44 production is involved in BYSMV infections.

To determine whether the two BYSMV P forms resulted from phosphorylation, we immunoprecipitated BYSMV P proteins from *N. benthamiana* leaves overexpressing *P* and treated the

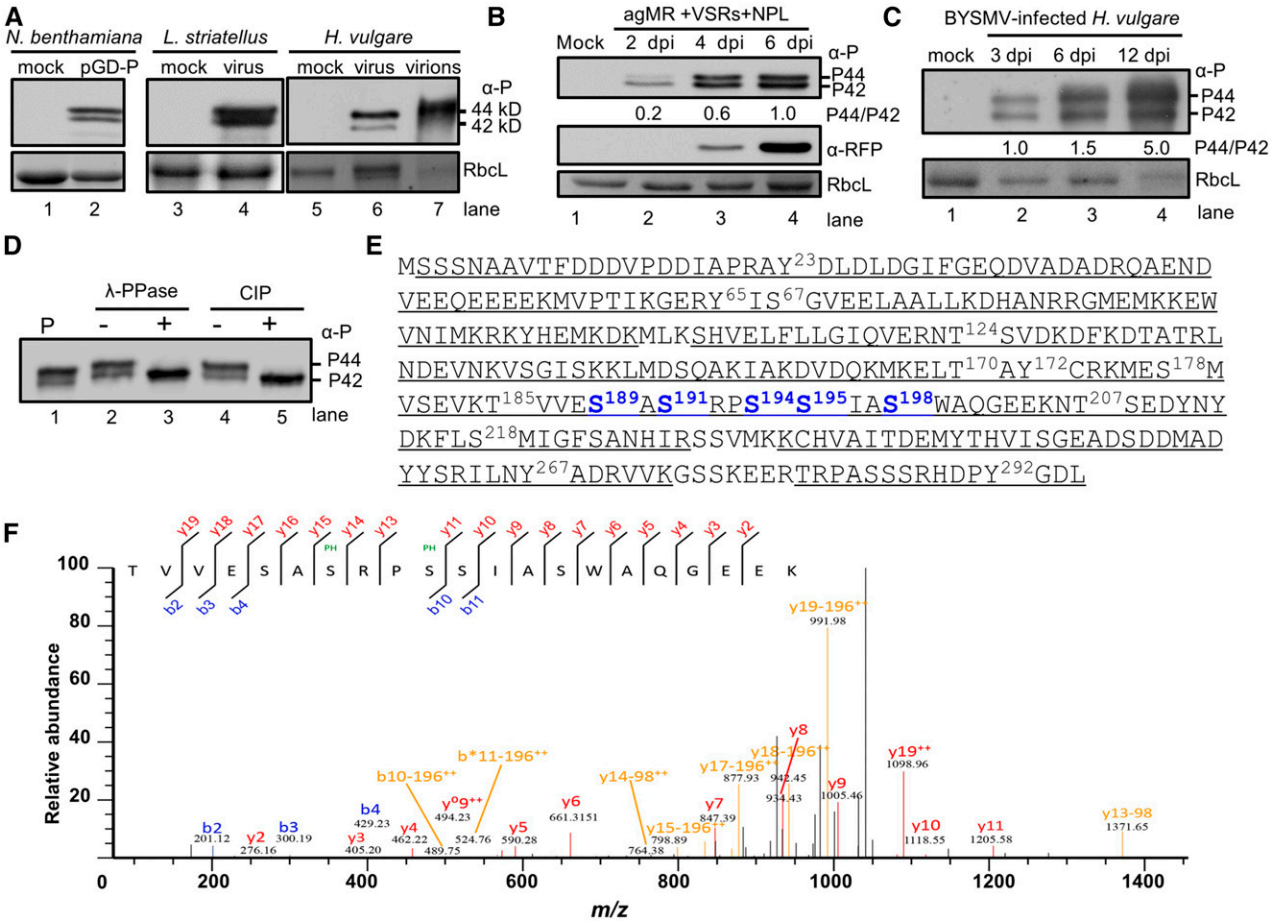

Figure 1. Identification of Phosphorylated Residues of BYSMV P by Mass Spectrometry.

(A) Immunoblot analysis showing two forms of the P protein expressed in *N. benthamiana*, *L. striatellus*, and *H. vulgare*, and purified virions, using specific antibodies against the P protein. Note the presence of two BYSMV P protein bands (P42 and P44) with molecular masses of 42 and 44 kD in gels.

(B) Accumulation of BYSMV P and RFP in agMR-inoculated *N. benthamiana* leaves at 2, 4, and 6 dpi. Total protein extracts from agMR-inoculated *N. benthamiana* leaves were probed with anti-P and anti-RFP antibodies. The P44:P42 ratios were calculated from band intensities.

(C) Accumulation of BYSMV P in BYSMV-infected *H. vulgare* plants at 3, 6, and 12 dpi. Coomassie Brilliant blue (CBB) staining of Rubisco complex large subunit (RbcL) was used as protein loading controls in **(A)** to **(C)**.

(D) Treatment of BYSMV P proteins with phosphatase. P-Flag proteins were isolated from *N. benthamiana* leaves infiltrated with the plasmid pMDC32-P by immunoprecipitation with anti-Flag beads. P-Flag proteins were treated with lambda protein phosphatase (λ-PPase) or CIP. Mock treatment (–) was incubated with buffer without phosphatases.

(E) Mass spectrometric identification of BYSMV protein phosphorylation sites. Underlined peptides (bold) were identified by mass spectrometry. The bold and numbered residues represent phosphorylation sites. Highly phosphorylated Ser residues of the BYSMV P protein SR motif are shown in blue.

(F) MS/MS spectrum of the peptide ^{185}TVVESASRPSSIASWAQGEEK^{205} containing the Ser-191 and Ser-194 phosphorylated residues. The b and y ions are highlighted in the sequence and corresponding labels in the spectrum.

immunoprecipitates with either λ-protein phosphatase or calf intestinal phosphatase (CIP). As expected, we failed to detect P44 after treatment with either phosphatase in vitro (Figure 1D), indicating that P42 and P44 represent hypo-phosphorylated and hyper-phosphorylated forms, respectively. In agreement with previous studies about the accumulation of animal rhabdovirus P proteins as two forms (Barik and Banerjee, 1992; Gupta et al., 2000), our results indicate that phosphorylation of BYSMV P similarly affects the mobility of P and phosphorylated P in SDS-PAGE gels.

To further identify phosphorylated residues in BYSMV P during replication and transcription, we immunoprecipitated the BYSMV P protein from BYSMV-agMR–infiltrated leaves and then subjected the protein samples to SDS-PAGE gel electrophoresis. We excised the P42 and P44 bands and treated them with trypsin for in-gel digestion. We analyzed the resulting products by liquid chromatography–tandem mass spectrometry (LC-MS/MS). The results showed that 95% of the BYSMV P protein was covered in the LC-MS/MS results from the P42 and P44 bands (Figure 1E), indicating that P42 is a full-length product rather than a truncated derivative. Notably, both P42 and P44 were characterized by different degrees of phosphorylation on a series of Ser, Thr, and Tyr residues (Figure 1E; Supplemental Table). Our LC-MS/MS results showed 17 phosphorylated Ser, Thr, and Tyr residues in 15 peptide fragments (Figure 1E; Supplemental Table). Notably, five Ser residues (amino acids 189, 191, 194, 195, and 198) in an SR motif (^{189}SASRPSSIAS^{198}) were highly phosphorylated in different peptides (Figures 1E and 1F; Supplemental Figure 1).

Collectively, the BYSMV P protein in plants and insect vectors exists as hyper-phosphorylation (P44) and hypo-phosphorylation (P42) forms in vivo. Moreover, the C terminus of BYSMV P contains a highly phosphorylated SR motif (Ser residues 189, 191, 194, 195, and 198).

Phosphorylation of the BYSMV P SR Motif Elicits P44 Production

IDRs have been described in numerous proteins required for various biological functions (Uversky et al., 2005). IDRs usually serve as flexible scaffolds for multi-component complex assemblies and exhibit different binding affinities to their partners (Spolar and Record, 1994; Wright and Dyson, 2009). Based on meta-prediction of IDRs from 15 independent predictors, we inferred that BYSMV P contained three structured domains, including an N-terminal domain (amino acids 9 to 33), a central domain (amino acids 60 to 183, and a C-terminal domain (amino acids 208 to 270), separated by two IDR regions, IDR^{N} (amino acids 34 to 59) and IDR^{C} (amino acids 184 to 207; Figure 2A). Interestingly, the highly phosphorylated SR motif (^{189}SASRPSSIAS^{198}) was located in the IDR^{C} region (amino acids 184 to 207; Figure 2A).

To examine whether phosphorylation of the BYSMV P SR motif affected conformational changes, we generated two BYSMV P mutants in which the five Ser residues at positions 189, 191, 194, 195, and 198 were substituted with Ala (designated as P^{S5A}) to mimic the nonphosphorylated state or with Asp (designated as P^{S5D}) to mimic the phosphorylated state (Figure 2A). We then expressed the wide-type P protein (P^{WT}), P^{S5A}, and P^{S5D} in *N. benthamiana* leaves by agro-infiltration. As described above, P^{WT} presented as both basally phosphorylated (P42) and hyper-phosphorylated (P44) forms (Figure 2B). By contrast, P^{S5A} and P^{S5D} migrated on SDS-PAGE gels only as P42 and P44, respectively (Figure 2B). These results indicate that BYSMV P phosphorylation (P^{S5D}) and nonphosphorylation (P^{S5A}) in the SR motif result in conformational changes that affect electrophoretic mobility of BYSMV P.

Effects of BYSMV P Phosphorylation on Minigenome Transcription and Replication

We recently developed a BYSMV-agMR system using a co-infiltration strategy in *N. benthamiana* leaves with Agrobacterium-harboring plasmids driving the accumulation of core proteins and a BYSMV anti-minigenome derivative cDNA (Fang et al., 2019). In the pBYSMV-agMR plasmid, we substituted the BYSMV N and P open reading frames (ORFs) from the antigenome strand with those of green fluorescent protein (GFP) and RFP flanked by the BYSMV 5′ and 3′ terminal sequences (Figure 2C). In addition, the infiltration system consisted of the pGD vector carrying the N, P, or L ORF from BYSMV (pGD-N, pGD-P, and pGD-L, respectively) and a pGD-VSRs plasmid that encodes the viral suppressors of RNA silencing p19 from tomato bushy stunt virus, γb from barley stripe mosaic virus, and P1/HC-Pro from tobacco etch virus (Figure 2C).

We next determined the effects of P mutants on BYSMV minigenome replication and transcription in vivo. We infiltrated Agrobacterium cultures containing plasmids for expression of P^{WT}, P^{S5A}, or P^{S5D} in *N. benthamiana* leaves along with mixtures of bacterial cultures harboring the pGD-N, pGD-L, pGD-VSRs, and agMR plasmids (Figure 2C). Compared to P^{WT}, the phosphorylation-deficient P^{S5A} mutant resulted in more GFP and RFP fluorescent foci, whereas the phospho-mimic variant P^{S5D} had the opposite effect (Figure 2D). In agreement, immunoblot analyses showed that P^{S5A} supported enhanced accumulation of GFP and RFP, whereas P^{S5D} caused a reduced accumulation of GFP and RFP, compared to P^{WT} (Figure 2E). As described above (Figure 2B), P^{WT} existed as the two forms P42 and P44, whereas P^{S5A} and P^{S5D} migrated with P42 and P44, respectively (Figure 2E).

We also performed a RNA gel blot analysis to measure BYSMV minigenome replication and associated transcription products. The RNAs corresponding to the genome- (gMR) and antigenomic-stranded (agMR) minigenome were the most abundant in P^{S5A}-infiltrated leaves, while they accumulated to intermediate levels in P^{WT}-infiltrated leaves and were the lowest in P^{S5D}-infiltrated leaves (Figure 2F). These results indicate that the replication of the minigenome is upregulated by P^{S5A} and downregulated by P^{S5D}. Quantification of band intensities from three independent experiments showed that accumulation of gMR in P^{S5A} samples increased threefold, whereas gMR in P^{S5D} only accumulated to 54% of P^{WT} levels (Figure 2G).

Next, we compared the transcriptional activities of P^{WT}, P^{S5A}, and P^{S5D} by detecting *GFP* mRNA. Since replicating minigenomes are templates for viral transcription, a rise in viral replication should positively affect viral transcription. We had therefore expected to see higher transcription in the P^{S5A} samples than in P^{WT} or P^{S5D}. However, P^{S5A} supported much lower *GFP* transcription than

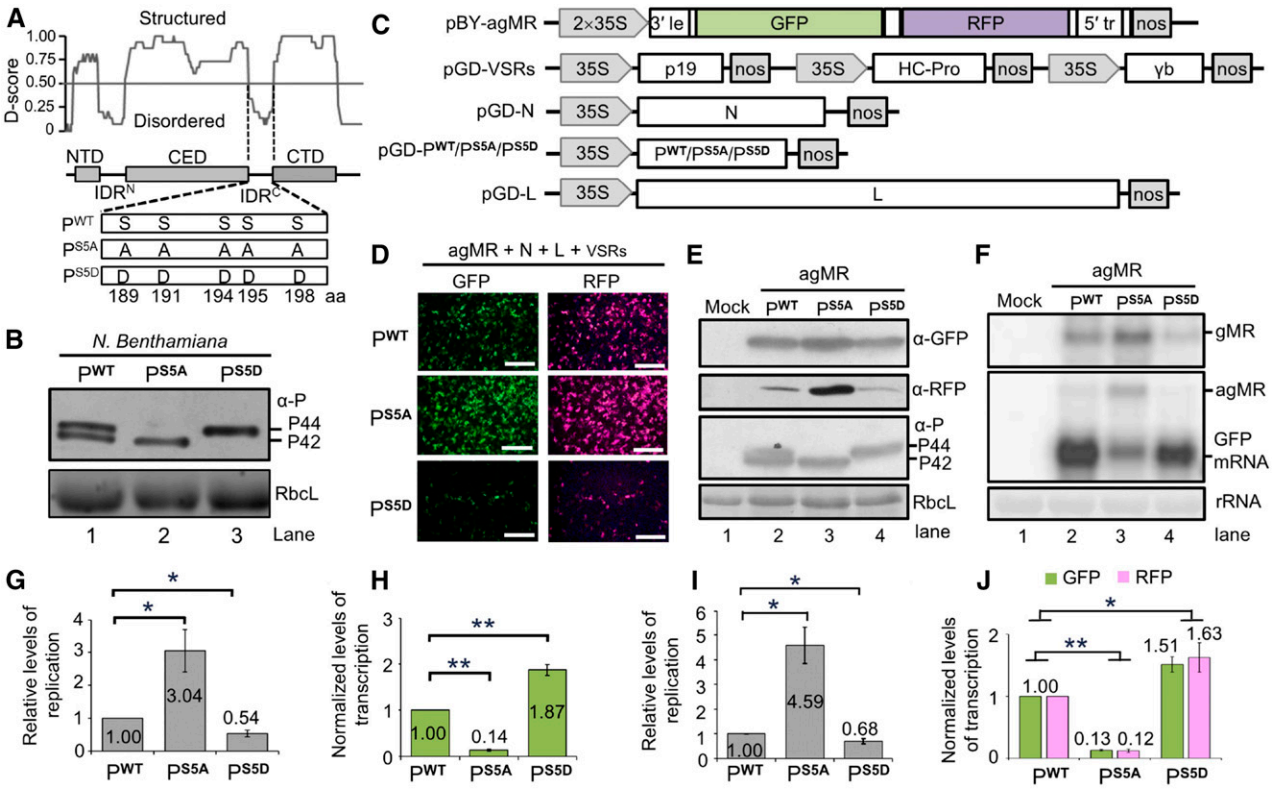

Figure 2. Effects of P Phosphorylation on Minigenome Transcription and Replication.

(A) Modular organization of the BYSMV P protein and schematic representation of its phosphorylation mutants. Normalized scores for disorder (D-score) were calculated from 15 different predictors as described in Methods. Structured regions and disordered regions are indicated by gray boxes and lines, respectively. Five Ser residues (amino acids 189, 191, 194, 195, and 198) in the SR motif of P^{WT} were mutated to either Ala (P^{S5A}) or to Asp (P^{S5D}).

(B) Immunoblot analyses of P^{WT}, P^{S5A}, and P^{S5D} levels in infiltrated leaves.

(C) Illustration of the binary vectors used for generating antigenomic-sense minireplicon RNA (pBY-agMR) and pGD constructs for expression of the BYSMV N, P/P^{S5A}/P^{S5D}, and L proteins in Agrobacterium-infiltrated *N. benthamiana* leaves. The pGD-VSRs plasmid contains three expression cassettes for simultaneous expression of the viral suppressors of RNA silencing TBSV p19, TEV HC-Pro, and BSMV γb.

(D) GFP and RFP foci in *N. benthamiana* leaves at 5 dpi with Agrobacterium cultures containing pBY-agMR, pGD-N, pGD-L, pGD-VSRs, and pGD-P/P^{S5A}/P^{S5D}. GFP and RFP was photographed with a fluorescence microscope. Bar = 1 mm.

(E) Immunoblot analysis showing GFP, RFP, and P expression in Agrobacterium-infiltrated leaves of **(D)** with anti-GFP (α-GFP), anti-RFP (α-RFP), and anti-P (α-P) polyclonal antibodies. Mock buffer-infiltrated leaves were used as negative controls.

(F) RNA gel blot analysis of M_R replication and transcription supported by P^{WT}, P^{S5A}, or P^{S5D} proteins in Agrobacterium-infiltrated leaves. rRNAs were used as loading controls.

(G) Relative levels of minigenome RNA replication calculated from signal intensities of gMR bands of **(F)**.

(H) Normalized levels of *GFP* mRNA transcription supported by the agMR plasmid in combination with the P^{WT}, P^{S5A}, or P^{S5D} proteins. Note: Normalized levels of transcription refer to the ratio between *GFP* mRNA accumulation and gMR accumulation.

(I) Quantification by qPCR of the relative levels of minigenome replication supported by the P^{WT}, P^{S5A}, or P^{S5D} proteins.

(J) *GFP* and *RFP* mRNA in the same agMR samples of **(I)** were analyzed by qPCR.

Note: All the results in **(G)** to **(J)** were obtained from three biologically independent experiments. The values in P^{WT} samples were set to 1. The *EF-1A* gene served as internal control in **(I)** and **(J)**. Error bars indicate SD. Data points above columns are mean values of three independent experiments. Statistically significant differences were determined by Student's *t* test. *P-value < 0.05; **P- < 0.01.

either P^{S5D} or P^{WT} (Figure 2F, *GFP* mRNA). To compare the transcriptional activities of these mutants, we normalized *GFP* transcript levels relative to the gMR template. Our results showed that P^{S5A} decreased transcriptional activity to only 14% of that observed with P^{WT}, whereas viral transcription with P^{S5D} increased by 87% over that seen with P^{WT} (Figure 2H).

To further verify the RNA gel blot results, we performed a real-time quantitative RT-PCR (RT-qPCR) analysis to quantify the levels of the minigenome RNA and *GFP*/*RFP* transcripts. Minigenome RNA levels were significantly upregulated in the P^{S5A} samples but were reduced in the P^{S5D} samples compared to the P^{WT} samples (Figure 2I). *GFP* and *RFP* transcript levels were significantly downregulated in P^{S5A} samples but were upregulated in P^{S5D} samples (Figure 2J), providing further support to our RNA gel blot results (Figures 2E to 2H).

We next mutated each Ser residue within the SR motif individually to Ala to determine the relative contribution of each Ser

residue during viral RNA synthesis. The Ser-191 (P^{S191A}), Ser-195 (P^{S195A}), and Ser-198 (P^{S198A}) single mutants resulted in similar numbers of fluorescent foci as P^{S5A} (Supplemental Figure 2A). By contrast, the P^{S189A} and P^{S194A} mutants had fewer fluorescent foci (Supplemental Figure 2A). Immunoblot analysis confirmed that the P variants P^{S191A}, P^{S195A}, P^{S198A}, and P^{S5A} all supported higher RFP accumulation than that seen with P^{S189A} or P^{S194A} (Supplemental Figure 2B, top). In addition, P^{S191A}, P^{S195A}, P^{S198A}, and P^{S5A} coelectrophoresed with the P42 form, while P^{S189A} and P^{S194A} existed as both P42 and P44 forms (Supplemental Figure 2B, middle). These results demonstrate that the P^{S191A}, P^{S195A}, or P^{S198A} single mutants each affect P protein conformation and functionally similar to P^{S5A}.

Taken together, our results clearly demonstrate that the non-phosphorylated form (P^{S5A}) of BYSMV P enhances virus replication, whereas the phosphorylated form (P^{S5D}) facilitates virus transcription. These results thus provide evidence that phosphorylation of the SR motif of BYSMV P modulates the balance between RNA replication and transcription.

Effects of BYSMV P Phosphorylation on Full-Length Virus Infection in *N. benthamiana* Leaves

We have previously demonstrated the rescue of infectious BYSMV from cloned full-length cDNAs in SBPHs and cereal plants (Gao et al., 2019). To examine the effects of BYSMV P phosphorylation on virus infections, we generated a pGD-NLP^{S5A} mutant, based on the pGD-NLP^{WT} plasmid, that contains expression cassettes for the BYSMV N, P^{S5A}, and L core proteins (Figure 3A). In addition, we inserted point mutations into BYSMV-GFP (BYG) carried by the pBYG-P^{WT} plasmid to create pBYG-P^{S5A} and pBYG-P^{S5D} mutant versions of the full-length antigenome BYSMV cDNA containing a *GFP* gene insertion, as described previously by Gao et al. (2019; Figure 3A).

We achieved BYG-P^{S5A} infection by infiltration with Agrobacterium cultures harboring the pGD-VSRs, pGD-NLP^{S5A}, and pBYG-P^{S5A} binary vectors into *N. benthamiana* leaves. Similarly, we coexpressed the pGD-VSRs, pGD-NLP^{WT}, and pBYG-P^{WT} plasmids to rescue the wild-type BYG-P^{WT}. Compared to BYG-P^{WT}, the BYG-P^{S5A} mutant resulted in more fluorescent foci in infiltrated leaves, although their fluorescence intensity was much weaker (Figure 3B, top). RT-qPCR analysis showed that accumulation of the BYG-P^{S5A} gRNA was 1.9-fold higher than that of BYG-P^{WT}, whereas the BYG-P^{S5A} transcription levels were ~60% lower than those seen for BYG-P^{WT} (Figure 3C). These results indicate that P^{S5A} facilitates full-length virus replication but inhibits virus transcription.

We further compared the replication and transcription levels of BYG-P^{S5A} and BYG-P^{S5D} when coexpressed with NLP^{S5A}. BYG-P^{S5A} infection resulted in increased numbers of foci but lower fluorescence intensity for GFP compared to BYG-P^{S5D} infection (Figure 3B, bottom). In addition, BYG-P^{S5D} infections led to an ~60% reduction in replication but a twofold increase in transcription relative to BYG-P^{S5A} (Figure 3D). Immunoblot analyses revealed that NLP^{S5A}/BYG-P^{S5A} only produced the P42 form, whereas the NLP^{WT}/BYG-P^{WT} and NLP^{S5A}/BYG-P^{S5D} combinations resulted in the production of both P42 and P44 forms (Supplemental Figure 3). The detection of the BYSMV M protein accumulation by immunoblot indicates that all combinations supported virus infection and were able to rescue recombinant BYSMV-GFP in *N. benthamiana* leaves (Supplemental Figure 3).

Collectively, these results indicate that the P^{S5A} mutant facilitates replication, while the P^{S5D} mutant assists in transcription during infections with full-length BYSMV virus genome, which is consistent with the agMR assays (Figure 2).

Effects of BYSMV P Phosphorylation on BYSMV Transmission by SBPHs

BYSMV is transmitted to cereal plants by SBPHs in a persistent-propagative manner (Cao et al., 2018). Our recent studies have demonstrated the successful infection of SBPHs by injection with crude extracts of *N. benthamiana* leaves containing recombinant BYSMV-GFP (Gao et al., 2019). Since P^{WT} can produce both P42 and P44 in vivo, we generated pBYG-P$^{S5A/S5D}$ and pBYG-P$^{S5D/S5A}$ constructs to coexpress P^{S5A} and P^{S5D} in full-length virus infections (Figure 4A).

To determine the effects of P phosphorylation on SBPH infection and transmission, we injected SBPHs with crude extracts of the *N. benthamiana* leaves infiltrated with BYG-P^{WT}, BYG-P^{S5A}, BYG-P^{S5D}, BYG-P$^{S5A/S5D}$, or BYG-P$^{S5D/S5A}$ (Supplemental Figure 4A). At 9 dpi, we observed faint GFP fluorescence from SBPHs infected with BYG-P^{WT}, BYG-P$^{S5A/S5D}$, or BYG-P$^{S5D/S5A}$ leaf extracts, but not in SBPHs injected with BYG-P^{S5A} or BYG-P^{S5D} extracts (Figure 4B). By 15 dpi, more than 45% of the SBPHs infected with BYG-P^{WT}, BYG-P$^{S5A/S5D}$, or BYG-P$^{S5D/S5A}$ exhibited intense GFP fluorescence. By contrast, only 0.30% of all SBPHs injected with BYG-P^{S5A} or BYG-P^{S5D} extracts exhibited very faint GFP fluorescence (Figures 4B and 4C). Immunoblot analyses revealed that BYG-P^{WT}, BYG-P$^{S5A/S5D}$, and BYG-P$^{S5D/S5A}$ infections resulted in similar accumulation of GFP, N, and P proteins (Figure 4D). These results demonstrate that both P^{S5A} and P^{S5D} are required for efficient BYSMV infections in SBPHs.

Next, we transferred SBPHs that had been infected with BYG-P^{WT}, BYG-P$^{S5A/S5D}$, and BYG-P$^{S5D/S5A}$ to healthy barley plants (five insects per plant) for a 2-d inoculation access period (IAP). Approximately 15 d after the inoculation access period, we detected GFP fluorescence in ~46% of newly emerging leaves of BYG-P^{WT}–infected barley plants (Figure 4E). However, none of the barley plants exhibited GFP fluorescence after being fed to BYG-P$^{S5A/S5D}$– or BYG-P$^{S5D/S5A}$–infected SBPHs (Figure 4E), indicating that neither BYG-P$^{S5A/S5D}$ nor BYG-P$^{S5D/S5A}$ in SBPHs were transmitted to barley plants by SBPHs.

Collectively, these results suggest that both P^{S5A} and P^{S5D} are essential for the dissemination of BYSMV in SBPHs. Nonetheless, coexpression of P^{S5A} and P^{S5D} in SBPHs is not sufficient for BYSMV transmission to barley plants. Therefore, the transmission of BYG-P^{WT} by SBPHs may require spatial- and temporal-specific expression of P42 and P44, rather than coexpression of P42 and P44.

BYSMV P Phosphorylation Mutants Have Different Association for the N–RNA Complex and L Protein

In rhabdovirus replication and transcription complexes, the P protein is involved in increasing (1) the solubility of the N protein

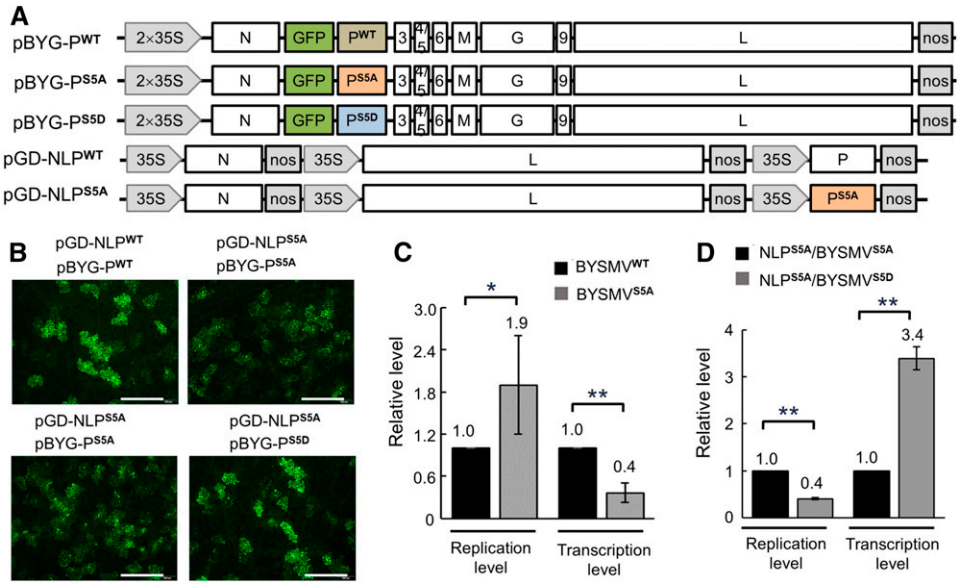

Figure 3. Effects of P Protein Phosphorylation on Full-Length BYSMV Transcription and Replication in *N. benthamiana* Leaves.

(A) Illustration of BYSMV genome organization and the binary Agrobacterium vectors harboring pBYG-P^{WT}, pBYG-P^{S5A}, pBYG-P^{S5D}, pGD-NLP^{WT}, and pGD-NLP^{S5A}.

(B) GFP foci in *N. benthamiana* leaves at 10 dpi with Agrobacterium cultures containing the indicated plasmids. GFP fluorescence was observed and photographed with a fluorescence microscope. Bar = 0.5 mm.

(C) Relative replication and transcription levels of recombinant $BYSMV^{WT}$ and $BYSMV^{S5A}$ as quantified by RT-qPCR. $BYSMV^{WT}$ was rescued by co-infiltration of pGD-NLP^{WT} and pBYG-P^{WT}, while $BYSMV^{S5A}$ was rescued by coinfiltration of pGD-NLP^{S5A} and pBYG-P^{S5A}. The values of viral replication and transcription supported by $BYSMV^{WT}$ were set to 1.

(D) Relative replication and transcription levels of recombinant $BYSMV^{S5A}$ and $BYSMV^{S5D}$ as quantified by RT-qPCR. $BYSMV^{S5A}$ and $BYSMV^{S5D}$ were rescued by coinfiltration of pBYG-P^{S5A} and pBYG-P^{S5D} under the support of pGD-NLP^{S5A}. The values of viral replication and transcription supported by $BYSMV^{S5A}$ were set to 1.

In **(C)** and **(D)**, error bars indicate SD. Data points above the columns are the mean values of three independent experiments. Statistically significant differences were determined by Student's *t* test. *P-value < 0.05; **P-value < 0.01.

and (2) the attachment of the L protein subunit to the N–RNA template. Because the BYSMV P SR motif is located in a highly disordered region, we hypothesized that the phosphorylation state within the SR motif might affect the binding of P protein to the N–RNA template and/or the L protein. To test this hypothesis, we performed biomolecular fluorescence complementation (BiFC) assays and coimmunoprecipitation (Co-IP) assays to investigate the binding of P mutants with N–RNA templates and the L protein.

BiFC and Co-IP assays demonstrated that full length P^{WT}, P^{S5A}, and P^{S5D} exhibited similar interaction with the BYSMV N^0 protein (Supplemental Figures 5A and 5B). In addition, the point mutations did not affect the self-interactions of full-length P^{WT}, P^{S5A}, and P^{S5D} (Supplemental Figures 5C and 5D). The N and C termini of rhabdovirus P proteins affect how P binds to RNA-free N^0 and to N–RNA templates (Leyrat et al., 2011). Thus, to prevent the binding of the P protein with N^0, we deleted the N-terminal 101 amino acids of P^{WT}, P^{S5A}, and P^{S5D}, while the remaining C termini were tagged with the N-terminal half (Y^N) of yellow fluorescent protein (YFP). We tagged the BYSMV N protein with the C-terminal half (Y^C) of YFP. In addition, as a negative control, we fused ribulose-1,5-bisphosphate carboxylase/oxygenase (Rubisco) with Y^C and Y^N individually. We observed no BiFC fluorescence in Rubisco control samples that were coexpressed with $P^{WT\Delta N101}$-Y^N, $P^{S5A\Delta N101}$-Y^N, $P^{S5D\Delta N101}$-Y^N, or N-Y^C (Supplemental Figure 6). However, after coexpression of N-Y^C with $P^{WT\Delta N101}$-Y^N, $P^{S5A\Delta N101}$-Y^N, or $P^{S5D\Delta N101}$-Y^N, we detected many punctate granules in the cytoplasm (Figure 5A). Leaves coinfiltrated with $P^{S5D\Delta N101}$-Y^N and N-Y^C had far fewer granules than in leaves coinfiltrated with N-Y^C and either $P^{WT\Delta N101}$-Y^N or $P^{S5A\Delta N101}$-Y^N (Figures 5A and 5B), suggesting that P^{S5D} has a lower binding affinity to the N–RNA template than P^{WT} and P^{S5A}.

To further examine the association of P mutants with N–RNA in vivo, we performed Co-IP assays using N–RNA complexes and Agrobacterium-infiltrated leaves expressing Flag-tagged P^{WT}, P^{S5A}, or P^{S5D} and anti-Flag beads. A mutant bearing a deletion of the C-terminal 120 residues ($P^{\Delta C120}$) that does not contain the N–RNA complex binding domain served as a negative control. We isolated the BYSMV N–RNA complexes from detergent-treated purified virus using a standard protocol of high-salt incubation and double isolation on a cesium chloride (CsCl) gradient (Emerson and Yu, 1975). Immunoblot and RT-PCR analyses showed that BYSMV N protein and gRNA were present in the purified N–RNA complexes within the nucleocapsid complexes (Supplemental Figure 7). Flag-P^{WT} and Flag-P^{S5A} efficiently immunoprecipitated BYSMV N proteins from the N–RNA complexes (Figure 5C, lanes 7 and 8). By contrast, Flag-P^{S5D} immunoprecipitated much less N

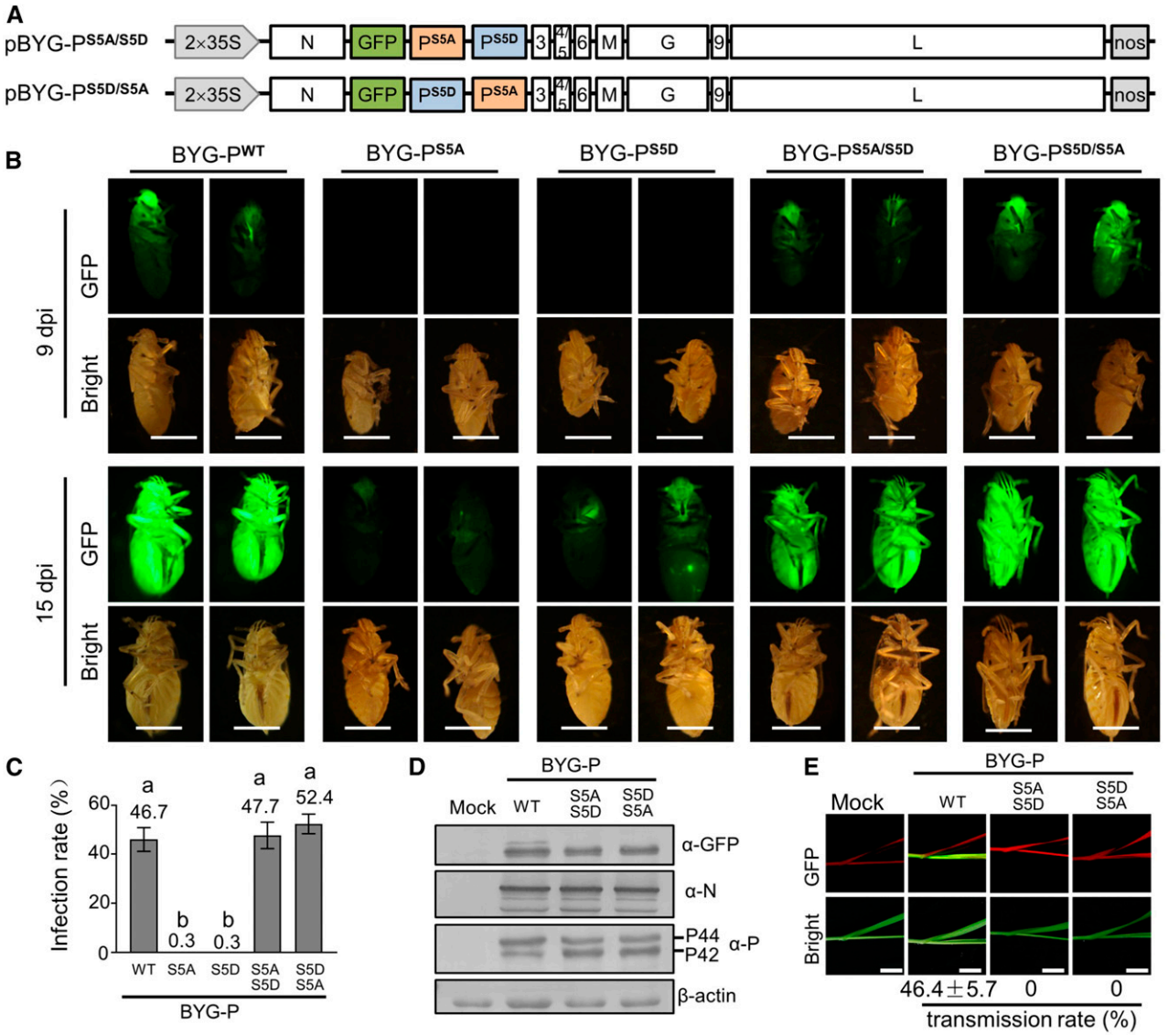

Figure 4. Effects of P Phosphorylation on Full-Length Virus Transcription and Replication in Planthopper Vectors.

(A) Illustration of the genome organization of the pBYG-$P^{S5A/S5D}$ and pBYG-$P^{S5D/S5A}$ binary vectors harbored by the Agrobacterium cultures.

(B) GFP fluorescence of SBPHs microinjected with crude extracts of *N. benthamiana* leaves infected by BYG-P^{WT}, BYG-P^{S5A}, BYG-P^{S5D}, BYG-$P^{S5A/S5D}$, and BYG-$P^{S5D/S5A}$ at 9 and 15 dpi. Bar = 1 mm.

(C) Infection rates ($n \geq 30$) of BYG-P^{WT}, BYG-P^{S5A}, BYG-P^{S5D}, BYG-$P^{S5A/S5D}$, and BYG-$P^{S5D/S5A}$ in SBPHs. Data are based on three independent experiments. Error bars indicate SD. Data points above the columns represent mean values of three independent experiments. Different letters indicate significant differences (ANOVA, $P < 0.001$).

(D) Immunoblot analysis of GFP, N, and P accumulation in SBPHs infected by BYG-P^{WT}, BYG-$P^{S5A/S5D}$, and BYG-$P^{S5D/S5A}$ with anti-GFP (α-GFP), anti-N (α-N), and anti-P (α-P) polyclonal antibodies. The SBPH β-actin protein served as a loading control.

(E) GFP fluorescence in systemically infected barley leaves at 15 d after feeding with SBPHs infected by BYG-P^{WT}, BYG-$P^{S5A/S5D}$, or BYG-$P^{S5D/S5A}$. Photographs were taken with a digital camera under a hand-held UV lamp. The values under the photos represent the mean infection rates of three independent experiments. Error bars indicate SD. Bar = 1 cm.

protein from the purified N–RNA complexes (Figure 5C, lane 9). Flag-GFP and Flag-$P^{\Delta C120}$ were unable to immunoprecipitate N from the purified N–RNA complexes (Figure 5C, lane 10). Thus, these results show that the P^{S5D} mutant exhibits compromised association with the N–RNA complex.

We next examined the binding between the P protein mutants and the L protein in Co-IP assays with Agrobacterium-infiltrated *N. benthamiana* leaves coexpressing L-6×Myc and Flag-tagged GFP, P^{WT}, P^{S5A}, or P^{S5D}. Both the Flag-P^{WT} and Flag-P^{S5D} proteins, but not the Flag-GFP control, efficiently immunoprecipitated

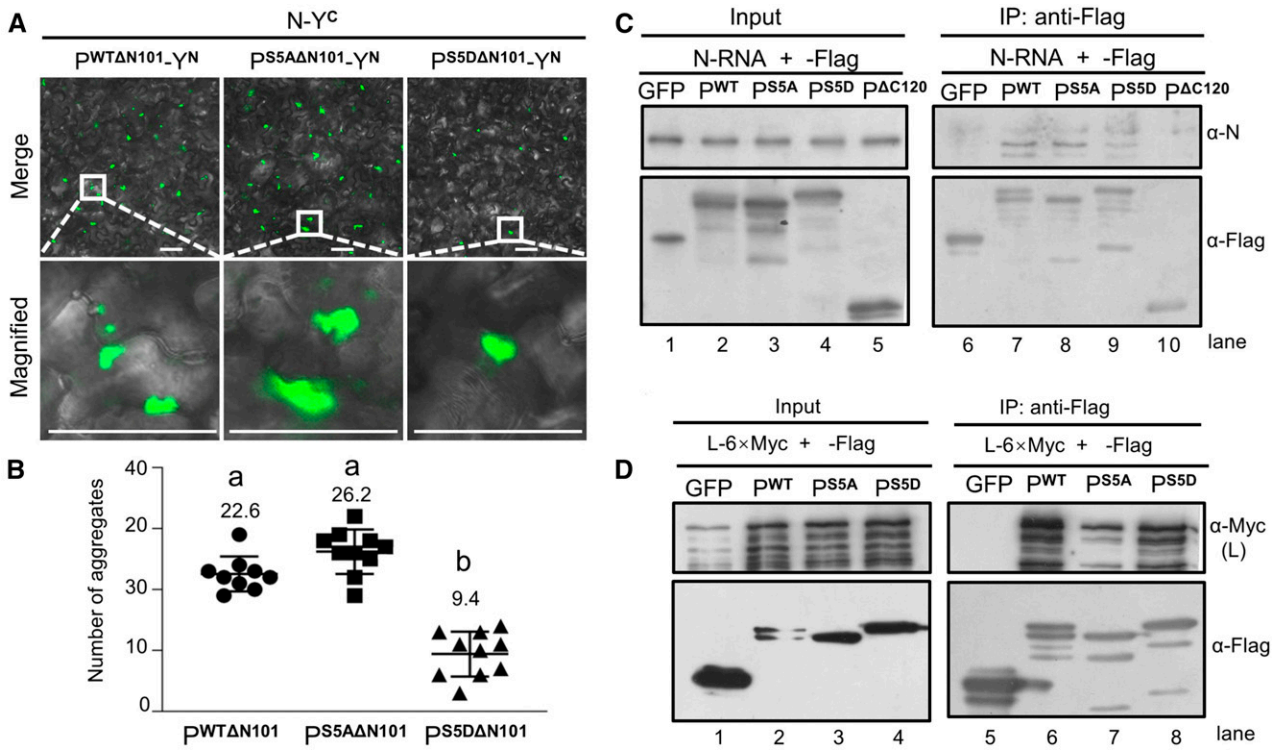

Figure 5. Association of BYSMV P^{S5A} and P^{S5D} With N–RNA Templates and the L Protein.

(A) BiFC detection of interactions between $P^{WT}/P^{S5A}/P^{S5D}$ and the N–RNA complexes. *N. benthamiana* leaves were photographed at 3 dpi, after infiltration with Agrobacterium cultures harboring plasmids encoding N-Y^C with $P^{WT\Delta N101}$-Y^N, $P^{S5A\Delta N101}$-Y^N, or $P^{S5D\Delta N101}$-Y^N. Y^N and Y^C represent the N-terminal and C-terminal halves of YFP, respectively. Bar = 50 μm.

(B) Quantification of the number of fluorescent aggregates in **(A)**. Each data point represents the number of fluorescent aggregates in a single photograph. Error bars indicate SD. Letters indicate significant differences (ANOVA, $P < 0.001$).

(C) Co-IP assays showing in vivo interactions between the $P^{WT}/P^{S5A}/P^{S5D}$ proteins and purified N–RNA complexes. Flag-tagged $P^{WT}/P^{S5A}/P^{S5D}$ proteins were expressed in and precipitated from *N. benthamiana* leaves with Flag M2 beads at 3 dpi. The N–RNA complexes were isolated from purified virions. The N (α-N) and Flag (α-Flag) antibodies were used to detect accumulation of N–RNA or P, respectively. GFP-Flag or $P^{\Delta C120}$-Flag served as negative controls.

(D) Co-IP assays showing $P^{WT}/P^{S5A}/P^{S5D}$ protein interacting with L. Flag-tagged $P^{WT}/P^{S5A}/P^{S5D}$ and L-6×Myc were coexpressed in *N. benthamiana* leaves and Co-IPed with anti-Flag beads at 3 dpi. Protein levels was detected by immunoblot using α-Flag and α-Myc antibodies. GFP-Flag and L-Myc were coexpressed as negative controls.

L-6×Myc (Figure 5D, lanes 6 and 8). By contrast, the Flag-P^{S5A} protein immunoprecipitated L-6×Myc with a reduced efficiency despite equal protein amounts in the starting samples (Figure 5D, lanes 3 and 7).

Collectively, we conclude that the P^{S5A} variant mimicking the nonphosphorylated state of P associates strongly with N–RNA templates and weakly with the L protein. Conversely, the phosphorylation mimic P^{S5D} mutant is compromised in the N–RNA template interaction. Therefore, the nonphosphorylated and phosphorylated states of the SR motif drive P protein conformational changes, thereby forming different complexes to initiate either transcription or replication.

The SR Motif of BYSMV P Is Phosphorylated by Plant and Insect CK1 Proteins

Phosphorylation is a universal posttranslational modification in all eukaryotes, including yeasts, animals, and plants. Therefore, we expressed the BYSMV P protein in yeast (*Saccharomyces cerevisiae*, strain BY4741) to determine whether BYSMV P could be phosphorylated by yeast protein kinases. Indeed, yeast-expressed BYSMV P also electrophoresed as P42 and P44, which match the migration pattern of P^{S5A} and P^{S5D}, respectively (Supplemental Figure 8). These results indicate that one or more conserved protein kinase(s) might be responsible for phosphorylating BYSMV P in host both plants and insect vectors. Therefore, we explored conserved protein kinases and constructed a phylogenetic tree using multiple sequence alignment tools (Supplemental Figure 9). In the yeast proteome, we identified 47 protein kinases that were highly conserved in barley plants and planthoppers (Supplemental Figure 9, labeled in red). We cloned 16 protein kinase genes from yeast to test their kinase activity against the BYSMV P protein.

Since eukaryotic-type protein kinases are absent in *Escherichia coli*, we modified a bacterial coexpression system to screen kinase candidates easily through the coexpression of individual protein kinases and their candidate target in *E. coli* (Heger-Stevic

et al., 2018). The BYSMV P protein expressed alone in *E. coli* only produced the P42 form, indicating that protein kinases targeting BYSMV P are absent in *E. coli* (Supplemental Figure 10A, lane 1). We then coexpressed BYSMV P with our 16 yeast protein kinase candidates in *E. coli.* Immunoblot analyses revealed that BYSMV P migrated as both the P42 and P44 forms only when coexpressed with the yeast kinase HO and Radiation Repair25 (HRR25; Supplemental Figure 10A, lane 13). By contrast, coexpression of the glutathione S-transferase (GST) fusion protein GST-HRR25 did not change the mobility of P^{S5A}, indicating that the Ser residues of the SR motif were phosphorylated by HRR25 (Supplemental Figure 10B). Furthermore, the GST-HRR25–generated P44 form disappeared after treatment with CIP, confirming that P44 was the hyper-phosphorylated form (Supplemental Figure 10C).

The yeast kinase HRR25 belongs to the CK1 family. BLAST searches showed that the *N. benthamiana*, SBPHs, and barley genomes encode 14, 5, and 14 yeast CK1 orthologs, respectively (Supplemental Figure 11). We next evaluated the effects of representative probable CK1 orthologs from *N. benthamiana* (*Nb*CK1), barley (*Hv*CK1), and planthoppers (*Ls*CK1) on the phosphorylation of BYSMV P in *E. coli*. Coexpression of *Nb*CK1.3, *Nb*CK1.4, *Nb*CK1.7, and *Nb*CK1.13 resulted in the conversion of P42 to P44 (Supplemental Figure 12), but these kinases had no effect on P^{S5A} mobility, as expected (Supplemental Figure 12). Using a similar strategy, we established that *Ls*CK1.3, *Ls*CK1.4, *Hv*CK1.2, *Hv*CK1.3, and *Hv*CK1.12 phosphorylated P^{WT} but had no effect on P^{S5A} in *E. coli* (Supplemental Figure 12). Therefore, these results suggest that CK1 orthologs in plants and insect hosts contribute to phosphorylation of the BYSMV P SR motif.

We selected *Nb*CK1.3, *Ls*CK1.3, and *Hv*CK1.3 for further analysis. *Nb*CK1.3, *Ls*CK1.3, and *Hv*CK1.3 resulted in the accumulation of the hyper-phosphorylated P44 form of P when coexpressed with BYSMV P^{WT} (Figure 6A, lanes 2 to 4), but had no effect on the mobility of BYSMV P^{S5A} (Figure 6A, lanes 6 to 8). Moreover, the P44 derivatives produced by *Nb*CK1.3, *Ls*CK1.3, and *Hv*CK1.3 disappeared after CIP treatment (Figure 6B, lanes 6 to 8), indicating that P44 is hyper-phosphorylated. To further confirm that CK1-type kinases are responsible for BYSMV P phosphorylation in plants, we transiently expressed BYSMV P in *N. benthamiana* leaves and then treated the Agrobacterium-infiltrated leaves with 50 μM D4476, a specific CK1 inhibitor, or with DMSO alone as solvent control (Rena et al., 2004). Immunoblot analyses revealed that the D4476 treatment significantly inhibited the accumulation of P44 compared to the DMSO control treatment (Figure 6C, cf. lanes 2 and 3). Moreover, P44 production was significantly induced by overexpression of *Nb*CK1.3 relative to the empty vector control (Figure 6C, cf. lanes 4 and 5). These results indicate that CK1 phosphorylates the SR motif of BYSMV P in vivo.

To verify BYSMV P phosphorylation in vitro, we purified P-6×His, P^{S5A}-6×His, GST-GFP, GST-*Nb*CK1.3, and GST-*Ls*CK1.3 recombinant proteins from *E. coli* for in vitro phosphorylation assays with [γ-^{32}P]ATP. In control experiments, we detected no radiolabel after incubation of GST-GFP with P-6×His or P^{S5A}-6×His (Figure 6D, lanes 1 and 4). The incubation of P-6×His with GST-*Nb*CK1.3 or GST-*Ls*CK1.3 generated radiolabeled phosphorylated P-6×His (Figure 6D, lanes 2 and 3). By contrast, radiolabeled phosphorylated P^{S5A}-6×His products significantly decreased in the presence of GST-*Nb*CK1.3 or GST-*Ls*CK1.3, as expected (Figure 6D, lanes 5 and 6). Collectively, these results indicate that the Ser residues (Ser-189, Ser-191, Ser-194, Ser-195, and Ser-198) of the SR motif are phosphorylated by host CK1 kinases in vivo and in vitro.

BYSMV P Recruits NbCK1.3 into Viroplasm-Like Bodies

Since CK1 can phosphorylate the BYSMV P protein, we hypothesized that BYSMV P may interact with CK1 within the viroplasm-like bodies that include the N, P, and L core proteins. To test this hypothesis, we performed GST pull-down assays to determine whether P and *Nb*CK1.3 interact. Indeed, GST-*Nb*CK1.3, but not GST-GFP, was immunoprecipitated with P-6×His in vitro (Figure 6E). To visualize the association of P with *Nb*CK1.3 in living cells, we conducted BiFC assays in *N. benthamiana* leaves. In agreement with the pull-down assays, coexpression of both Y^N-P/Y^C-NbCK1.3 and Y^C-P/Y^N-NbCK1.3 resulted in fluorescent granules in the cytoplasm of infiltrated cells (Figure 6F). Notably, these granules trafficked rapidly throughout the cytoplasm (Supplemental Movies 1 and 2). By contrast, we observed no BiFC fluorescence in the control samples, in which Rubisco was coexpressed with P or *Nb*CK1.3 fused with different Y^N and Y^C (Supplemental Figure 13).

BiFC of Y^N-P/Y^C-NbCK1.3 and Y^C-P/Y^N-NbCK1.3 resulted in trafficking granules that were reminiscent of the BYSMV P-mediated viroplasm-like bodies seen in our recent work (Fang et al., 2019). We therefore coexpressed L-mCherry and CFP-N with the BiFC combinations of Y^N-P/Y^C-*Nb*CK1.3 and Y^C-P/Y^N-*Nb*CK1.3. Satisfyingly, L-mCherry and CFP-N colocalized with the trafficking granules formed by the interaction of Y^N-P/Y^C-*Nb*CK1.3 with Y^C-P/Y^N-*Nb*CK1.3 (Figure 6G; Supplemental Movies 3 and 4). These results suggest that *Nb*CK1.3 is recruited by BYSMV P to form trafficking viroplasm-like bodies in which BYSMV P can be efficiently phosphorylated by NbCK1.3.

RNA Interference against CK1 Inhibits Efficient Infection of BYSMV in SBPHs

Our results thus far show that host CK1 interacts with BYSMV P and phosphorylates the SR motif of BYSMV P (Figure 6), indicating that CK1 plays important roles in BYSMV infections. To obtain genetic confirmation of this hypothesis, we synthetized a 600-bp double RNA fragment (ds*LsCK1*) corresponding to the homologous region between *LsCK1.3* and *LsCK1.4* in vitro to reduce the expression of *LsCK1.3* and *LsCK1.4* in SBPHs. We coinjected the thoraxes of *L. striatellus* with crude extracts of BY-GFP–infected barley plants and either ds*LsCK1* or ds*Amp* (ampicillin, 70 ng per insect) as a negative control. At 5 dpi, ds*LsCK1*-treated insects exhibited much lower GFP fluorescence signal than ds*Amp*-injected insects (Figure 7A). In agreement, immunoblot analyses revealed that GFP, N, and P proteins also accumulated to a lower level in ds*LsCK1*-treated insects than in ds*Amp*-injected insects (Figure 7B, compare lanes 2 and 3).

RT-qPCR analyses further revealed that BY-GFP gRNA levels decreased by ~58% in ds*LsCK1*-treated SBPHs compared with ds*Amp*-injected SBPHs (Figure 7C). Moreover, *LsCK1.3* and *LsCK1.4* in the ds*LsCK1*-treated insects decreased by ~72 and

48%, respectively (Figure 7D). Collectively, these results suggest that knocking down *LsCK1* transcript levels negatively affects virus infections in SBPHs.

Overexpression of CK1 and a Dominant-Negative Mutant Impairs BYSMV Infections in Plants

To investigate whether CK1 affects BYSMV infections in plants, we overexpressed *Nb*CK1 proteins by placing their coding regions under the control of the cauliflower mosaic virus 35S promoter with the agMR systems. Unfortunately, coinfiltrated leaves exhibited cell death in the infiltrated patches (Supplemental Figure 14A), which would affect the agMR replication. To avoid the appearance of cell death, we used an estrogen-inducible promoter to drive the expression of plant *CK1* genes in *N. benthamiana* leaves. In these experiments, we treated coinfiltrated leaves with 2 μM estradiol at 3 dpi, before subjecting them to trypan blue staining and observation for RFP foci 2 d later.

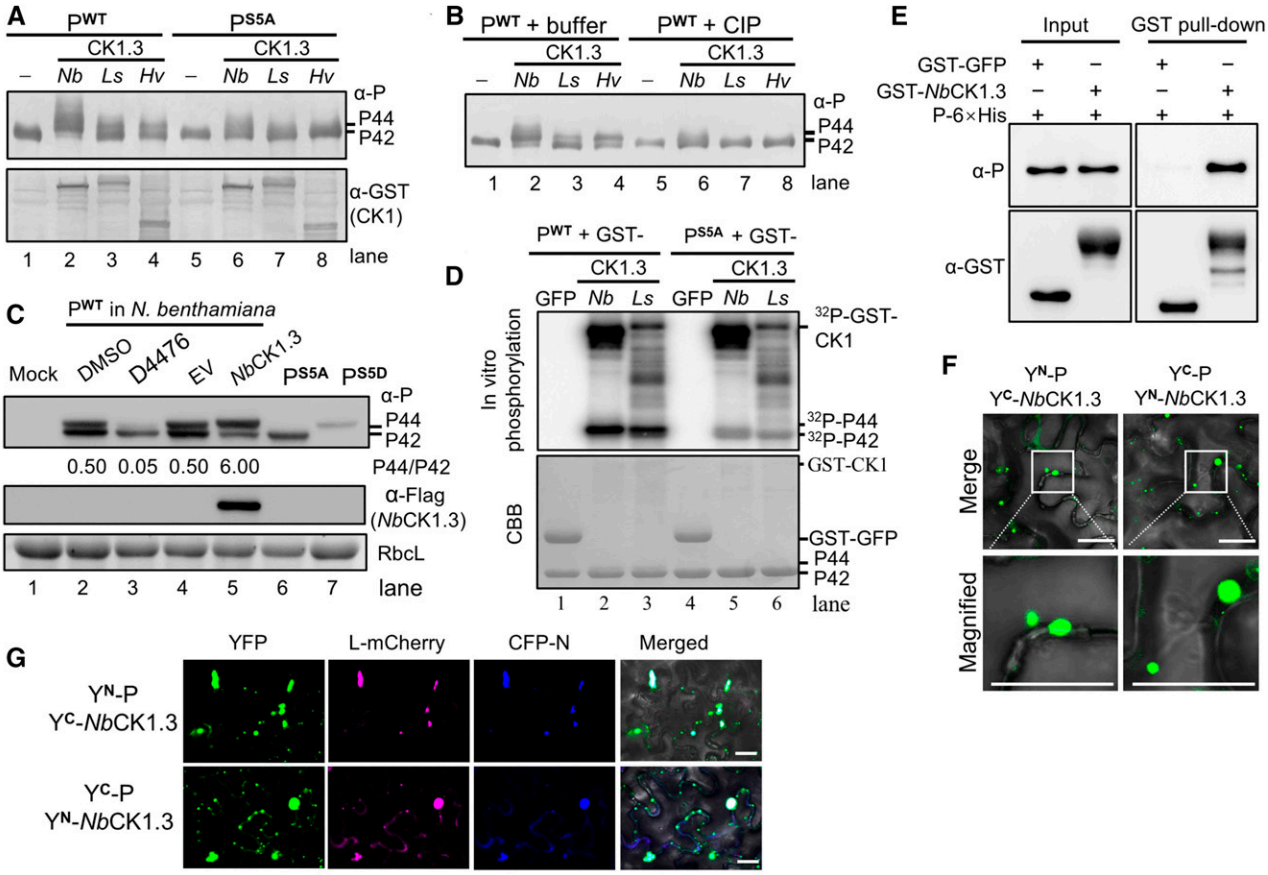

Figure 6. CK1 Phosphorylates the SR Motif of BYSMV P.

(A) Detection of the phosphorylation forms of P^{WT} and P^{S5A} expressed alone (–) or with *Nb*CK1.3, *Ls*CK1.3, and *Hv*CK1.3 in *E. coli*. The anti-P and anti-GST polyclonal antibodies were used to detect accumulation of P and protein kinases, respectively.

(B) Treatment with CIP affects the forms of BYSMV P. Purified P^{WT}-6×His proteins were treated with buffer or CIP and then analyzed by immunoblot analysis.

(C) Accumulation of the two forms of BYSMV P^{WT} after transient expression in *N. benthamiana* leaves. Infiltrated leaves were treated with DMSO buffer (lane 2) or the CK1-specific inhibitor D4476 (lane 3) at 2 dpi and collected for P protein detection at 3 dpi. Infiltrated leaves coexpressing P^{WT} with empty vector (EV) or *Nb*CK1.3 were collected for P protein detection at 3 dpi. P^{S5A} and P^{S5D} from Agrobacterium-infiltrated *N. benthamiana* leaves served as P protein phosphorylation markers.

(D) Autoradiograph showing in vitro [γ-^{32}P]ATP phosphorylation of the SR motif of BYSMV P by *Nb*CK1.3 and *Ls*CK1.3. Recombinant GST-*Nb*CK1.3 and GST-*Ls*CK1.3 proteins purified from *E. coli* were used as protein kinases. GFP-GST acted as a negative control. The purified P^{WT}-6×His and P^{S5A}-6×His proteins from *E. coli* served as substrates. Autophosphorylated CK1 and phosphorylated P are indicated. Coomassie Brilliant blue (CBB)–stained gels served as protein loading controls.

(E) Pull-down assays showing physical interactions between BYSMV P-6×His and GST-*Nb*CK1.3 in vitro. GST-GFP was used as a negative control.

(F) BiFC assays showing the association between BYSMV P and *Nb*CK1.3 in *N. benthamiana* leaves. The photographs were taken at 3 dpi. The N-terminal and C-terminal halves of YFP are designated Y^N and Y^C. Bar = 20 μm.

(G) Colocalization of BYSMV L and N with punctate particles formed by BiFC assay of P and *Nb*CK1.3. L-mCherry and CFP-N were coexpressed with Y^N-P and Y^C-*Nb*CK1.3 or Y^C-P and Y^N-*Nb*CK1.3 combinations in *N. benthamiana* leaves, respectively. Fluorescence images were photographed at 3 dpi. Bar = 20 μm.

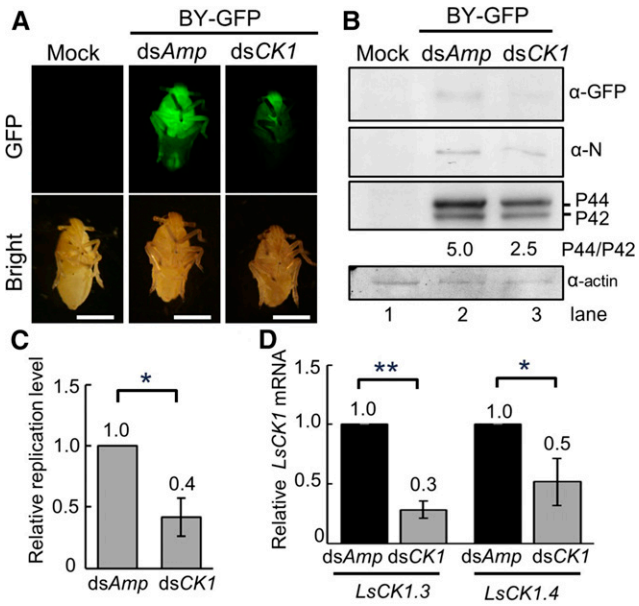

Figure 7. Knocking Down CK1 Expression Suppresses BYSMV Infection of SBPHs.

(A) GFP fluorescence in SBPHs microinjected with crude extracts of BYG-P–infected barley leaves with the ds*Amp* or ds*CK1* RNAs at 5 dpi. Bar = 1 mm.

(B) Immunoblot analysis showing accumulation of the GFP, N, and P proteins in the samples of **(A)**. The SBPH β-actin protein served as a loading control.

(C) RT-qPCR analysis showing relative replication levels of BYSMV in the samples of **(A)**.

(D) RT-qPCR analysis showing accumulation of *LsCK1.3* and *LsCK1.4* in the samples shown in **(A)**. The viral replication values with *LsCK1.3* and *LsCK1.4* in the ds*Amp*-treated SBPHs were set to 1. In **(C)** and **(D)**, error bars indicate SD. Data points are mean value of three independent experiments. Statistically significant differences were determined by the Student's *t* test. *P-value < 0.05; **P-value < 0.01.

Estradiol-induced expression of *CK1* did not cause cell death in the infiltrated patches (Figure 8A). Compared to the empty vector control, coexpression of *Nb*CK1.3 with P^{WT} greatly decreased the numbers of RFP foci (Figure 8B, top). Notably, coexpression of *Nb*CK1.3 also reduced the accumulation of the P42 form (Figure 8C), indicating that *Nb*CK1.3 phosphorylated the P^{WT} protein in vivo. Accumulation of the RFP protein and genomic minireplicon RNA (gMR) decreased in the samples overexpressing *Nb*CK1.3 (Figures 8C and 8D). By contrast, coexpression of *Nb*CK1.3 did not affect the P^{S5A}-mediated improvement in agMR replication (Figures 8A and 8B). In these assays, *Nb*CK1.13 was also coexpressed with P^{WT}, which improved P44 production and inhibited agMR replication in *N. benthamiana* leaves (Supplemental Figure 15). Collectively, these results indicate that overexpression of CK1 negatively regulates BYSMV infections through phosphorylation of the P SR motif.

Dominant-negative approaches have been used to inhibit endogenous CK1 activity in mammalian cells (Zhu et al., 1998; Lee et al., 2009). The point mutants CKIε (K38R) and CKIα (D136N) were used as dominant-negative mutants in previous studies by Zhu et al. (1998) and Lee et al. (2009). Protein blast showed that the K38 of CKIε and D136 of CKIα are also conserved in plant CK1 homologs (K38 and D128; Supplemental Figure 14B). Accordingly, we generated the point mutant (K38R and D128N) in *Hv*CK1.2 to serve as a dominant-negative mutant, *Hv*CK1.2^{DN} (Supplemental Figure 14B). Unlike the wild-type *Hv*CK1.2, HvCK1.2^{DN} did not induce cell death in *N. benthamiana* leaves due to its lack of kinase activity (Supplemental Figure 14A). Moreover, coexpression of *Hv*CK1.2^{DN} interfered with its phosphorylation of the BYSMV P protein (Supplemental Figure 14C).

We next generated a recombinant BYSMV plasmid containing *Hv*CK1.2^{DN} (pBY-GFP-*Hv*CK1.2^{DN}) based on pBY-GFP, which would drive the accumulation of GFP to act as a visual marker of systemic BYSMV infections in barley plants (Figure 8E). Following rescue in *N. benthamiana* leaves and transmission by SBPHs, BY-GFP and BY-GFP-*Hv*CK1.2^{DN} established systemic infections in barley plants at 10 dpi (Figure 8F). BY-GFP spread extensively in the first fully expanded leaves of infected plants, whereas BY-GFP-*Hv*CK1.2^{DN} was limited to several veins (Figures 8F and 8G). Immunoblot analysis showed that GFP accumulated to much lower levels in BY-GFP-*Hv*CK1.2^{DN}–infected leaves than BY-GFP (Figure 8H). To ensure the clear detection and differentiation of the P42 and P44 bands, we diluted BY-GFP total protein samples 10 times for immunoblot analysis. As hoped, overexpression of the dominant-negative mutant (*Hv*CK1.2^{DN}) reduced the ratio of P44 to P42 compared with that of BY-GFP (Figure 8H). In agreement, RT-qPCR results showed that the accumulation of gRNA in BY-GFP-*Hv*CK1.2^{DN}–infected leaves decreased to 22% of that seen with BY-GFP (Figure 8I). As a control for infection assays, we replaced *Hv*K1.2^{DN} from BY-GFP-*Hv*CK1.2^{DN} with the *β-GLUCURONIDASE* (*GUS*) gene to generate BY-GFP-GUS. Similarly to BY-GFP, BY-GFP-GUS exhibited higher pathogenicity than BY-GFP-*Hv*CK1.2^{DN} in barley plants (Supplemental Figure 16). Collectively, these results indicate that overexpression of CK1.2^{DN} inhibits BYSMV infections in barley plants.

In summary, our results demonstrate that CK1 proteins from plant and insect vectors can phosphorylate the BYSMV P protein and induce transition from virus replication to transcription (Figure 8J). The phosphorylated P44 form facilitates virus transcription, whereas the nonphosphorylated P42 form improves virus replication (Figure 8J). Since both virus replication and transcription are required for effective virus infection, either inhibition or overexpression of host CK1 genes impair the balance between virus replication and transcription, thereby inhibiting BYSMV infections (Figure 8).

DISCUSSION

Phosphorylation of cellular proteins is a widespread post-translational modification that regulates signal transduction, molecular interactions, and subcellular localization phenomena (Peck, 2006; Bond et al., 2011). Viral proteins are usually phosphorylated by host protein kinases that play pivotal roles in viral life cycles (Jakubiec and Jupin, 2007; Wang, 2015). Here, we have identified two phosphorylated states of the BYSMV P protein that represent the hypo-phosphorylated (P42) and the hyper-phosphorylated (P44) forms (Figure 1). In this respect, the BYSMV P protein is similar to the *Rabies virus* (RV) P protein, which

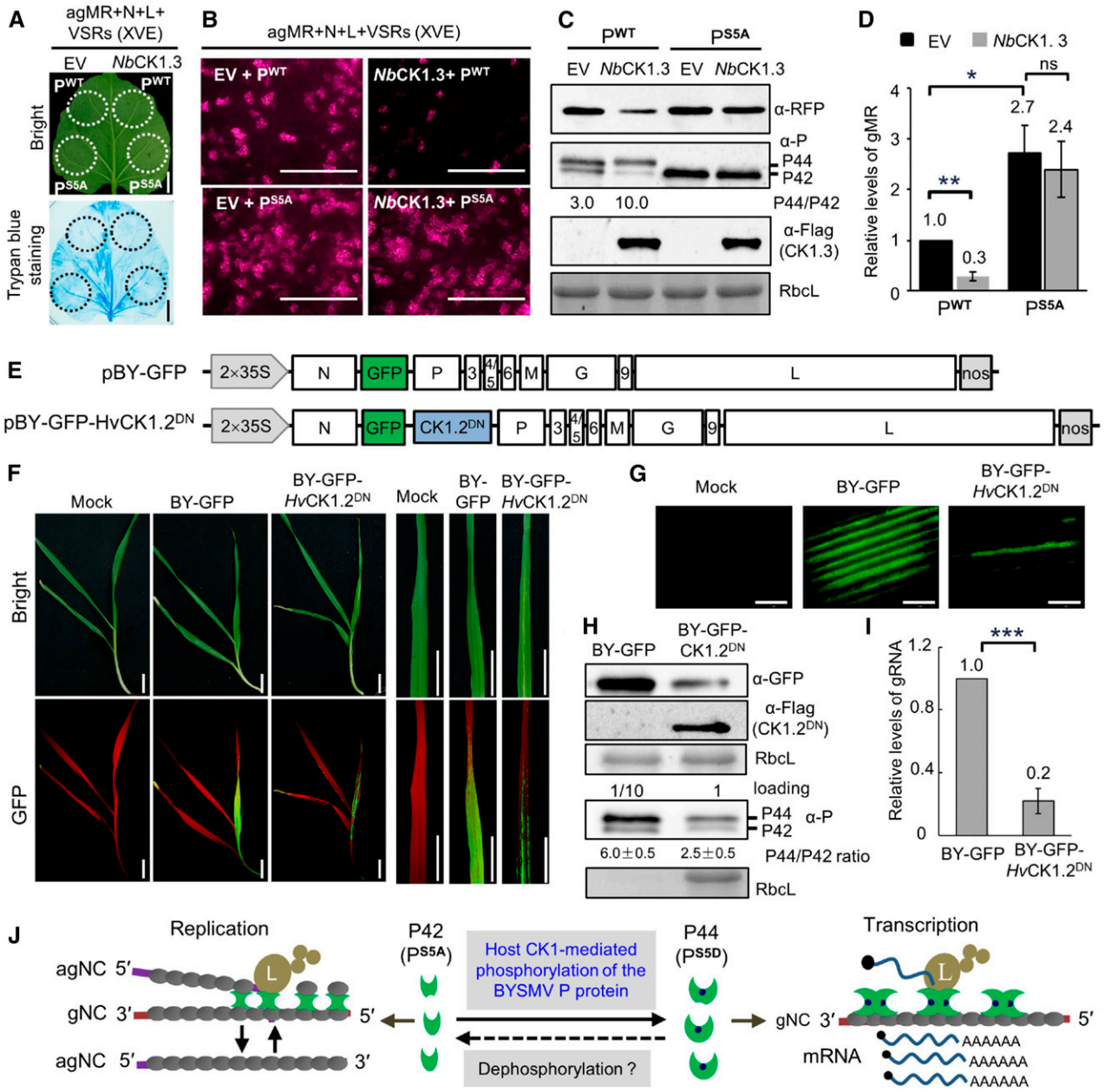

Figure 8. Overexpression of CK1 Suppresses BYSMV Infections in Plants.

(A) Trypan blue staining of *N. benthamiana* leaves at 5 dpi after infiltration with Agrobacterium cultures containing pBY-agMR, pGD-N, pGD-L, pGD-VSRs, and pGD-P^{WT} (wild type)/P^{S5A} (phosphorylation defective mutant) with empty vector (EV) or *Nb*CK1.3 under the control of the estradiol-inducible promoter. Estradiol (2 μM) was infiltrated at 3 dpi, and the leaves were stained at 5 dpi. Bar = 2 cm.

(B) RFP foci in *N. benthamiana* leaves from **(A)** at 5 dpi. Bar = 1 mm.

(C) Immunoblot analysis showing accumulation of the RFP, P, and *Nb*CK1.3 proteins in the samples of **(B)**. RbcL served as a loading control.

(D) RT-qPCR analysis showing accumulation of gMR in the samples shown in **(B)**.

(E) Illustration of the genome organization of the pBY-GFP and pBY-GFP-HvCK1.2^{DN} binary vectors harbored by the Agrobacterium cultures.

(F) Disease symptoms and GFP fluorescence of barley plants infected with BY-GFP and BY-GFP-*Hv*CK1.2^{DN} at 15 dpi. Bar = 2 cm.

(G) GFP foci in barley leaves of **(F)** observed by confocal microscope. Bar = 1 mm.

(H) Immunoblot analysis showing accumulation of the GFP and *Hv*CK1.2^{DN} proteins in the samples of **(F)**. For detection of the BYSMV P protein, the total protein samples of BY-GFP were diluted 10 times for immunoblot analysis. RbcL served as a loading control.

(I) RT-qPCR analysis showing accumulation of BYSMV gRNA in the samples shown in **(F)**.

has both a basally phosphorylated and a hyper-phosphorylated form (Tuffereau et al., 1985; Takamatsu et al., 1998). However, the protein kinases catalyzing the phosphorylation of the RV P protein remain elusive. Here, we discovered that host CK1 protein kinases are responsible for BYSMV P phosphorylation and P44 production (Figure 6). Furthermore, multiple CK1 orthologs phosphorylated BYSMV P protein in *N. benthamiana*, planthoppers (*L. striatellus*), and barley (Supplemental Figure 12). BYSMV infections of barley plants did not induce expression of these *CK1* genes (Supplemental Figure 17), possibly because normal *CK1* levels are sufficient for the phosphorylation of BYSMV P. It is important to note that BYSMV is a cross-kingdom virus infecting both plants and insects. Correspondingly, CK1 is a well-conserved kinase family in eukaryotes, including dicot and monocot plants, as well as in SBPHs (Knippschild et al., 2005); thus, it is not surprising that CK1 plays an important role in the cross-kingdom life cycle of BYSMV in plants and insect vectors.

Another interesting finding in our study is that the Ser-rich region (SR motif) of the BYSMV P protein was highly phosphorylated (Figure 1). Using site-directed mutants and phosphorylation assays in *E. coli* and in vitro, we clearly show that the SR motif is phosphorylated by host CK1 (Figure 6). Furthermore, the nonphosphorylated P^{S5A} mutant of the SR motif only migrates as P42, whereas the phospho-mimic mutant P^{S5D} exists as P44 in SDS-PAGE gels (Figure 2B), suggesting that the phosphorylated and nonphosphorylated SR motifs drive conformational changes between the two forms (P42 and P44). More interestingly, the SR motif is located in the C-terminal IDRs of the BYSMV P protein. Many IDRs with increased flexibility usually serve as scaffolds for the assembly of functional complexes involved in cell signaling, molecular recognition, and regulation processes (Uversky et al., 2005). Thus, our results strongly suggest that host CK1-mediated SR phosphorylation changes the flexibility of the BYSMV P C-terminal IDR to mediate conformational changes from P42 to P44. Moreover, the conformational changes between P42 and P44 result in different complexes for optimal replication or transcription. We have therefore provided evidence showing that a host kinase can target the C-terminal IDR region of a rhabdovirus P protein and affect viral RNA replication and transcription.

Rhabdovirus transcription and replication are executed by the same polymerase complexes and are finely regulated in a dynamic balance (Ivanov et al., 2011). An intriguing question is how viral polymerase complexes are finely regulated to initiate either transcription or replication. Using our recent BYSMV reverse genetics systems, we showed that the nonphosphorylated mutant (P^{S5A}) of the SR motif increased replication but reduced transcription. Conversely, the P^{S5D} variant, which mimics the P-phosphorylated form, stimulates transcription and inhibits replication (Figure 2). It should be noted that P^{S5D}-induced transcripts were based on significantly reduced gMR templates, which probably led to aberrant transcripts with no coding capacity. Therefore, it is not surprising that P^{S5D} supported higher accumulation of *GFP* mRNA but reduced the accumulation of GFP protein than P^{S5A} (Figures 2E and 2F). Collectively, our results demonstrate that the phosphorylation states of the SR motif modulate the balance between viral replication and transcription in vivo. Several pioneering studies using *Vesicular stomatitis virus* (VSV) minigenome systems have demonstrated that N- or C-terminal phosphorylation of the VSV P protein affects RNA replication or transcription (Hwang et al., 1999; Chen et al., 2007, 2013; Mondal et al., 2014). For instance, CK2 phosphorylates the N terminus of the VSV P protein and affects P oligomerization, which is required for virus transcription rather than replication (Pattnaik et al., 1997; Qanungo et al., 2004). Here, the IDR^C motif of the rhabdovirus P protein is a new phosphorylated domain, which affects both virus replication and transcription. It is striking to note that the P proteins of animal rhabdovirus RV and VSV, as well as plant cytorhabdovirus, such as *Northern cereal mosaic virus*, also contain SR motifs in their C-terminal IDR regions (Supplemental Figure 18; Gerard et al., 2009). Broader implications of our finding await investigations into whether the CK1 family is a common modulator of other plant and animal rhabdoviruses.

In the field, BYSMV is transmitted by SBPHs in a persistent-propagative manner (Cao et al., 2018), meaning that BYSMV is disseminated to plants solely by these insects, and its survival depends entirely on replication in SBPHs. Our results show that CK1 in SBPHs can phosphorylate the SR motif of the BYSMV P protein (Figures 1 and 6). Thus, the SBPH CK1 protein is instrumental in BYSMV infections. Indeed, knockdown of *LsCK1* by RNA interference significantly affected virus accumulation and dissemination (Figure 7). Using our full-length infectious clones, we clearly show that highly efficient replication and transcription supported by P^{S5A} and P^{S5D}, respectively, are essential for virus infection in SBPHs. Nonetheless, BYG-$P^{S5A/S5D}$ and BYG-$P^{S5D/S5A}$ failed to be transmitted to barley plants by the infected SBPHs. Thus, it remains to be determined whether spatial- and temporal-specific accumulation of P^{S5A} and P^{S5D} or other factors play a role during the different infection stages of BYSMV in SBPHs and barley plants.

In summary, the P44 hyper-phosphorylated form of the P protein is the principal product in BYSMV virus nucleocapsids (Figure 1A) and facilitates initiation of virus transcription from ribonucleoproteins (RNPs) released during the infection of cells. Subsequently, the freshly translated P42 form binds N^0 to form P–N^0 complexes and efficiently delivers the N^0 to the nascent RNA chains, which drives the switch from transcription to RNA

Figure 8. (continued).

(J) Proposed model for host CK1-mediated phosphorylation of the BYSMV P SR motif regulating virus transcription and replication. The BYSMV P proteins exist as a basally phosphorylated form (P42) and a hyper-phosphorylated form (P44). Viral replication and transcription of the N protein–encapsidated gRNA is accomplished by the polymerase L, P protein, and N proteins. The P protein dimer provides a physical link to attach the L protein to the N–RNA complex. Plant and insect CK1 proteins can phosphorylate the BYSMV P42 form to produce p44, which promotes the switch from replication to transcription.
In **(D)** and **(I)**, error bars indicate SD. Data points are mean value of three independent experiments. Statistically significant differences were determined by the Student's *t* test. *P < 0.05; **P < 0.01; ***P < 0.001.

replication. Upon phosphorylation of the P42 form by host CK1 proteins, the resulting P44 form exhibits compromised binding to N–RNA templates, which results in the dissociation of the complexes from N–RNA templates and the switch from gRNA replication to mRNA transcription (Figure 8J).

METHODS

Preparation of Host Plants and Insect Vectors

Nicotiana benthamiana and barley (*Hordeum vulgare* cv Golden promise) plants were cultivated in a growth room at 25°C with a 16-h-day/8-h-night cycle. SBPHs were initially isolated from Hebei Province, China, and reared in illumination incubators that were placed inside a climate chamber under a 16-h-d/8-h-night cycle at 26°C.

Virus Inoculation and Transmission

Virus recovery and transmission by SBPHs were performed as previously described by Gao et al. (2019) and Zhang et al. (2020). Briefly, the BYSMV infectious clones were transformed into Agrobacterium (*Agrobacterium tumefaciens*) strain EHA105. The bacteria were cultivated at 28°C for 12 h, harvested by centrifugation, and suspended in buffer (10 mM MES, 150 μM acetosyringone, and 10 mM $MgCl_2$). After incubation at 25°C for 3 h, bacterial suspensions were mixed and infiltrated in *N. benthamiana* leaves. At 14 dpi, inoculated leaves were homogenized in buffer (100 mM Tris-HCl, 40 mM Na_2SO_3, 10 mM Mg $(CH_3COO)_2$, and 1 mM $MnCl_2$, pH 8.4) and centrifuged at 12,000*g* for 15 min at 4°C. Crude extracts of infected *N. benthamiana* leaves (13.8 nL per insect) were injected into second-instar nymphs with a Nanoinject II auto-nanoliter injector (Drummond Scientific). After a 10-d incubation period, injected SBPH nymphs were transferred to healthy barley plants for a 2-d inoculation period. Observation of symptoms and virus analyses were performed at 10 to 15 dpi.

Plasmid Constructions

The pBYSMV-agMR, pGD-VSRs, pGD-N, pGD-P, pGD-L, and pGDG-P plasmids were previously described by Fang et al. (2019) as well as the pGD-NLP, pBY-GFP, and pBY-GR plasmids (Gao et al., 2019). We introduced the full-length P gene and the deletion fragment lacking the C-terminal 120 amino acids into plasmid pMDC32. The plasmids pMDC-P^{S5A} and pMDC-P^{S5D} were constructed by the Quick-Change mutagenesis method. The pGD-NLP^{S5A} was constructed by replacing the P coding sequence with P^{S5A} in the pGD-NLP plasmid. Based on the pBY-GFP construct that was used to design pBYG-P^{WT} (Gao et al., 2019), the fragment including P and P3 was PCR amplified and cloned into the pTOPO-Blunt vector to generate the pTO-BYP-P3 vector. For the recombinant virus plasmids pBYG-P^{S5A} and pBYG-P^{S5D}, the P^{S5A} and P^{S5D} coding sequence was PCR amplified and subcloned into the pTO-BYP-P3 vector, and the fragments including P^{S5A}-P3- or -P^{S5D}-P3 were PCR amplified and then substituted in place of the corresponding region of pBYG-P^{WT}. For pBYG-$P^{S5A/S5D}$ and pBYG-$P^{S5D/S5A}$, the RFP-P-P3 was PCR amplified from pBY-GR and subcloned into the M5 HiPer pTOPO-Blunt vector (Mei5 Biotechnology) to generate pTORFP-P-P3. The pTORFP-P^{S5A}-P3 and pTORFP-P^{S5D}-P3 plasmids were constructed by site-directed mutagenesis. Next, the RFP ORF of pTORFP-P^{S5A}-P3 and RFP-P^{S5D}-P3 were replaced with the P^{S5D} or P^{S5A} ORFs to generate pTO-$P^{S5D/S5A}$-P3 and pTO-$P^{S5A/S5D}$-P3, respectively. Finally, the $P^{S5D/S5A}$-P3 and $P^{S5A/S5D}$-P3 fragments were cloned into pBY-GR to generate pBYG-$P^{S5A/S5D}$ and pBYG-$P^{S5D/S5A}$. All primers used for these manipulations and other cloning experiments are listed in Supplemental Data Set 1.

Immunoblot Analysis

Agrobacterium-infiltrated *N. benthamiana* leaves were harvested at 2 to 6 dpi, and total proteins were extracted in SDS buffer (100 mM Tris, pH 6.8, 20% [v/v] glycerol, 4% [w/v] SDS, 0.2% [w/v] bromophenol blue, and 10% [v/v] β-mercaptoethanol) for immunoblot analysis. Proteins were separated on SDS-PAGE gels followed either by Coomassie Brilliant Blue R 250 staining or transfer onto nitrocellulose membranes for detection with polyclonal antibodies specific to the BYSMV N (1:5000), P (1:3000), GFP (1:2000), or RFP (1:2000) proteins. The antibodies of the BYSMV N, P, RFP, and GFP were acquired from rabbits immunized with prokaryotic expressed proteins as previously described by Fang et al., (2019) and Gao et al. (2019). Secondary reactions were performed with goat anti-rabbit IgG horseradish peroxidase conjugate (1:3000; catalog no. 1,706,515, Bio-Rad) and Pierce ECL Plus chemiluminescent substrate followed by exposure of the filters to x-ray films (Fujifilm).

Mass Spectrometric Analysis

Immunoprecipitation of Flag-tagged P protein and identification of phosphorylation sites by LC-MS/MS were performed as previously described by Hu et al. (2015). Briefly, soluble proteins were extracted from Agrobacterium-infiltrated *N. benthamiana* leaves and dissolved in immunoprecipitation (IP) buffer (25 mM Tris-HCl, pH 7.5, 150 mM NaCl, 10% [v/v] glycerol, 0.1% [v/v] Nonidet P-40, 2% [w/v] Polyvinylpyrrolidone 40, 1 mM NaF, 1mM $NaVO_3$, 1 mM EDTA, 10 mM DTT, and 1× protease inhibitor cocktail [Sigma-Aldrich]), followed by centrifugation at 10,000*g* for 30 min at 4°C. The supernatant was incubated with 20 μL of Flag-specific agarose beads at 4°C for 2 h. The immunoprecipitated Flag-P was washed five times with IP buffer and separated onto 12.5% (v/v) SDS-PAGE gels. After staining with the Plus Silver Stain Kit (Sigma-Aldrich), the Flag-P bands were cut out and subjected to in-gel trypsin digestion for 8 h at 37°C. The digested peptides were analyzed by Q-Exactive LC-MS/MS (Thermo Fisher Scientific) at the Mass Spectrometry Facility of China Agricultural University.

Meta-Prediction of IDRs

Disordered regions within the BYSMV P protein were predicted by submitting the amino acid sequence to 15 different predictors that perform well and are available through web servers. These include DisEMBL (Coils, Hotloops, and Remark465; Linding et al., 2003), DISpro (Obradovic et al., 2005), Spine-D (Zhang et al., 2012), Dispro (Cheng et al., 2005), IUPred (long and short; Dosztányi et al., 2005), Pdisorder (http://linux1.softberry.com/berry.phtml?topic=pdisorderandgroup=programsandsubgroup=propt), Poodle-S (Shimizu et al., 2007), Poodle-L (Hirose et al., 2007), PrDOS (Ishida and Kinoshita, 2007), Spritz (long and short; Vullo et al., 2006), and RONN (Yang et al., 2005). For each predicting algorithm, a score of 1 was attributed to each residue predicted to be in a structured region, whereas the predicted disordered residues were attributed a score of 0.

Phylogenetic Analysis

The CK1 protein sequences for *Saccharomyces cerevisiae*, *H. vulgare*, and *Laodelphax striatellus* were downloaded from different sources: *S. cerevisiae* kinases were downloaded from KinBase (http://kinase.com/web/current/), *H. vulgare* kinases from Ensembl Plants (plants.ensembl.org), and *L. striatellus* kinases from Gigadb (http://gigadb.org/data set/100361). The gene families of these three species were identified by the OrthoMCL v2.0.9 package (Li et al., 2003). We used each protein as a query against the Pfam database to identify their kinase domain. Phylogenetic analysis was conducted using MEGA7.0 (Kumar et al., 2016) followed by annotation with EvolView (He et al., 2016). For broad phylogenetic analysis of CK1 kinases in *N. benthamiana*, *L. striatellus*, and *H. vulgare*, we searched and

downloaded yeast protein HRR25 homologs in the three species using BLAST in the *N. benthamiana* Genome and Transcriptome database (https://sefapps02.qut.edu.au/blast/blast_link2.cgi), the *L. striatellus* protein databases (http://gigadb.org/data set/100361), and the barley protein database in Ensembl Plant (http://plants.ensembl.org/Multi/Tools/Blast?db=core). The phylogenetic trees were constructed using MEGA7.0.

Kinase Assays in *Escherichia coli*

We subcloned 16 yeast kinase genes in the prokaryotic expression vector pGEX-KG. Briefly, yeast kinase genes were queried in yeast databases (https://www.yeastgenome.org). The corresponding ORFs were amplified from yeast total RNA by RT-PCR and cloned into the pGEX-KG vector. For P^{WT} and P^{S5A} protein prokaryotic expression, the coding sequence was PCR amplified and cloned between the *Nde*I and *Xho*I restriction sites in pET-30a. To ensure coexpression of kinases and P protein in *E. coli*, the segments containing the -tac promoter-GST tag-kinase ORF- were PCR amplified and then fused with *Sph*I-linearized pET-P and pET-P^{S5A} to generate pET-P^{WT}-GST-Kinase and pET-P^{S5A}-GST-Kinase. The pET-P^{WT}-GST-Kinases and pET-P^{S5A}-GST-Kinases plasmids were transformed into *E. coli* (Rosetta strain) and induced by isopropyl β-D-1-thiogalactopyranoside (1 mM) for 8 h at 25°C. The *E. coli* cultures were harvested by centrifugation at 10,000*g* for 10 min at 25°C and extracted in SDS buffer (100 mM Tris, pH 6.8, 20% [v/v] glycerol, 4% [w/v] SDS, 0.2% [w/v] bromophenol blue, and 10% [v/v] β-mercaptoethanol) for immunoblot analysis with polyclonal antibodies against BYSMV P (1:3000) and GST (1:5000; GenScript, catalog no. A00866), respectively.

In Vitro Phosphorylation Assays

In vitro phosphorylation assays were performed according to previous studies by Hu et al. (2015) and Zhang et al. (2018). The pGEX-*Nb*CK1.3, pGEX-*Ls*CK1.3, pGEX-GFP, pET-P^{WT}, and pET-P^{S5A} plasmids were transformed into *E. coli* (Rosetta strain) and induced by isopropyl β-D-1-thiogalactopyranoside (0.3 mM) for 16 h at 18°C. GST-*Nb*CK1.3, GST-*Ls*CK1.3, and GST-GFP were purified by glutathione Sepharose 4 Fast Flow medium (GE Healthcare). The P^{WT}-6×His and P^{S5A}-6×His fusion proteins were purified by nickel-affinity agarose chromatography (Bio-Rad) according to the manufacturer's instructions. For in vitro phosphorylation assays, 0.1 μg of GST-*Nb*CK1.3, GST-*Ls*CK1.3, or GST-GFP was incubated for 30 min at 30°C with 1 μg of P^{WT}-6×His or P^{S5A}-6×His in 30 μL of 1× kinase buffer (25 mM HEPES, pH 7.5, 20 mM $MgCl_2$, 0.1 mg/mL BSA, 0.1 mM DTT, 0.1 mM ATP, and 0.3 μCi of [γ-^{32}P]ATP). Next, 5 μL of 5× SDS sample buffer was added to terminate the reactions. The proteins were separated on a 12.5% (v/v) SDS-PAGE gel, and the gel was dried using a model 583 Gel Dryer (Bio-Rad) for 45 min at 80°C. The phosphorylated P proteins were visualized via autoradiography.

The P-Flag protein immunoprecipitated from Agrobacterium-infiltrated *N. benthamiana* leaves or P^{WT} purified from *E. coli* was eluted from the resin by shaking for 1 h with IP buffer containing 0.1 mg/mL Flag peptide. The eluted P-Flag protein was incubated with 2 μL of 10 units/μL CIP (New England Biolabs) or 1 μL of 400 units/μL λ-protein phosphatase (New England Biolabs) in 50-μL reactions with protease inhibitor (1× cocktail; Roche) for 1 h at 37°C. Reactions were stopped by boiling them in gel loading buffer for immunoblot analysis with the anti-P antibody.

GST Pull-Down Assay

GST pull-down assays were performed as previously described by Yang et al. (2018). P-6×His proteins (~10 μg) were incubated at 4°C for 3 h with GST-GFP and GST-*Nb*CK1.3 proteins (~10 μg) in 600 μL of binding buffer (20 mM Tris-HCl, pH 7.5, 150 mM NaCl, 10% [v/v] glycerol, 0.2% [v/v] Triton X-100, 1 mM DTT, and 1× protease inhibitor cocktail) with 30 μL of glutathione Sepharose 4B beads (GE Healthcare). The beads were washed six times with binding buffer and eluted with 50 μL of binding buffer containing 10 mM reduced L-glutathione. The eluted fractions were boiled in equal volumes of 2× SDS loading buffer and then the proteins were analyzed by immunoblot with anti-GST (1:5000) and anti-P (1:3000) antibodies.

BYSMV-agMR Assays in *N. benthamiana* Leaves

BYSMV-agMR assays were performed as previously described by Fang et al. (2019). *N. benthamiana* plants with six to eight fully expanded leaves were used for BYSMV-agMR assays. Briefly, Agrobacterium harboring the pBYSMV-agMR (OD_{600} 0.3), pGD-VSRs (OD_{600} 0.1), pGD-N (OD_{600} 0.1), pGD-P (OD_{600} 0.1), and pGD-L (OD_{600} 0.3) plasmids were mixed and infiltrated into *N. benthamiana* leaves. Epidermal cells of infiltrated leaves were observed for GFP and RFP fluorescence at 6 dpi using a fluorescent microscope (model BX53; Olympus) or confocal laser scanning microscopy (model FV1000; Olympus).

RNA Gel Blots

For analysis of RNA synthesis in the BYSMV M_R system, total RNA was extracted from Agrobacterium-infiltrated *N. benthamiana* leaves using TRIzol reagent (Sigma-Aldrich). RNA gel blot detection of BYSMV M_R gRNA and agRNA derivatives and *GFP* mRNA was performed using 5 μg of total RNA as previously described by Dong et al. (2016). For gRNA or agRNA detection, the PCR fragments were obtained using pBYSMV agMR as a template with primers designed with T7 or SP6 promoters in the desired genomic or antigenomic orientations, followed by in vitro transcription with T7 or SP6 RNA polymerase in the presence of [^{32}P]UTP.

RT-qPCR

Total RNA isolated from MR-infiltrated leaves was treated with DNase I (Takara) to eliminate DNA contamination. Next, the treated total RNA (2 μg) was used as template for reverse transcription with oligo(dT) primer to detect mRNA or with B-RT-F and EF1a-R primers to detect minigenome RNA with Moloney Murine leukemia virus reverse transcriptase (Promega). RT-qPCR reactions were performed by amplifying *GFP* and *RFP* fragments to detect transcript levels and trailer fragments to monitor replication levels with SsoFast EvaGreen Supermix (Bio-Rad). The primers are listed in Supplemental Data Set 1. All RT-qPCR data were normalized to the *EF1a* gene. Three independent biological replicates were performed, each in technical triplicates, for statistical analysis as shown in Supplemental Data Set 2.

In Vivo Co-IP Assays

In vivo Co-IP assays were performed as previously described by Zhang et al. (2017b). *N. benthamiana* plants were infiltrated with Agrobacterium cultures for transient expression of recombinant proteins, and leaf tissues were homogenized in Co-IP buffer (25 mM Tris-HCl, pH 7.5, 150 mM NaCl, 10% [v/v] glycerol, 0.1% [v/v] Nonidet P-40, 2% [w/v] Polyvinylpyrrolidone 40, 1 mM NaF, 1 mM $NaVO_3$, 1 mM EDTA, 10 mM DTT, and 1× protease inhibitor cocktail [Sigma-Aldrich]). The supernatants produced by filtration and centrifugation (10,000*g* for 20 min at 4°C) were incubated for 2 h with anti-Flag M2 affinity beads (Sigma-Aldrich), followed by five washes with IP buffer. The immunoprecipitated products were boiled in SDS buffer for immunoblot assays with corresponding antibodies.

BiFC Assays

BiFC assays were performed as previously described by Zhang et al. (2017a), with minor modifications. The fragments of the BYSMV N, L, P, and P mutant were cloned into the BiFC vectors pSPYNE-35S and pSPYCE-35S with different primers listed in Supplemental Data Set 1. As control, the Rubisco coding sequence was cloned into the BiFC vectors (Zhang et al., 2017a). *N. benthamiana* leaves were coinfiltrated with Agrobacterium EHA105 cultures containing BiFC plasmids and the P19 viral suppressor plasmid at a final ratio of 0.2:0.2:0.1 (OD_{600}). The epidermal cells of Agrobacterium-infiltrated leaves were observed for fluorescence (YFP) using confocal laser scanning microscopy (model FV1000; Olympus).

N–RNA Purification by CsCl Gradient Centrifugation and In Vitro Co-IP

BYSMV-infected barley tissues were homogenized in buffer (0.3 M Gly and 0.1 M $MgCl_2$, pH 8.0), and the homogenates were filtered through two layers of gauze and centrifuged at 150*g* at 4°C for 5 min. The supernatant was mixed with chloroform (20% [v/v] final volume) and centrifuged at 1200*g* at 4°C for 20 min. The resulting aqueous supernatant was used for BYSMV RNP complex precipitation after addition of polyethylene glycol 6000 and NaCl to final concentrations of 6% and 3% (w/v), respectively, and centrifuged at 3500*g* at 4°C for 20 min. The pellet was resuspended in extraction buffer (100 mM Gly and 0.01 M $MgCl_2$, pH 7.0) and centrifuged at 160,000*g* for 90 min at 4°C in a Beckman L-80XP centrifuge, and N–RNA was purified from a portion of the BYSMV RNP as previously described by Zhang et al. (2013). BYSMV RNP pellets were also resuspended in 2 mL of CsCl buffer (10 mM Tris-HCl, pH 7.8, 150 mM NaCl, and 1 mM EDTA), loaded onto a discontinuous 25 to 40% (w/v) CsCl gradient (25%, 1.5 mL; 30%, 1.5 mL; and 40%, 1.5 mL) in dilution buffer (10 mM Tris-HCl, pH 7.8, 150 mM NaCl, and 1 mM EDTA), and centrifuged at 250,000*g* at 20°C for 1 h. The contents of the visible band were collected from the region between 30 and 40% (w/v) CsCl gradient and subjected to centrifugation at 200,000*g* at 4°C for 1 h. The resulting pellet was resuspended in 100 μL of 1× PBS for in vitro Co-IP. The purified N–RNA was divided into five equal aliquots and incubated with buffer containing Flag-tagged GFP, P^{WT}, P^{S5A}, P^{S5D}, and $P^{\Delta C120}$ immunoprecipitated from infiltrated *N. benthamiana* leaves with anti-Flag M2 affinity beads. Co-IP and immunoblot analyses were performed as described above.

CK1 Overexpression and Dominant-Negative Assays

The coding sequences of *NbCK.3*, *NbCK1.7*, *NbCK.13*, and *HvCK.12* were cloned into the pMDC32 vector for overexpression of CK1 in *N. benthamiana*. We induced expression of CK1 with estradiol according to a previous study by Zuo et al. (2000). Briefly, The *NbCK1.3* and *NbCK1.13* coding sequences were cloned into the pER8 vector to generate pER8-*Nb*CK1.3 and pER8-*Nb*CK1.13. Agrobacterium cultures harboring the pER8-*Nb*CK1.3/pER8-*Nb*CK1.13 and BYSMV-agMR systems plasmids were mixed and infiltrated into *N. benthamiana* leaves. Next, the infiltrated leaves were infiltrated with 2 μM estradiol at 3 dpi, and samples were collected at 5 dpi for RFP fluorescence observation and M_R replication analysis.

For CK dominant-negative assays, the *RFP* ORF of pBY-GR was replaced with *HvCK1.2* with two amino acid substitutions (K38R and D128N) or a GUS fragment to generate pBY-GFP-*Hv*CK1.2^{DN} or pBY-GFP-GUS. Next, the recombinant viruses were rescued from *N. benthamiana* to planthopper and then to barley as previously described by Gao et al. (2019). The accumulation of recombinant viruses in infected barley plants was evaluated with a hand-held blue green lamp (Luyor Instrument) and photographed with a Canon digital camera at 15 dpi.

Virus Inoculation, Double-Stranded RNA Injection, and Insect Transmission

Protocols for crude extraction of BYSMV virions from plant materials and injection into planthopper nymphs have been previously described by Gao et al. (2019). To determine virus transmission by planthoppers, injected nymphs were allowed to feed on healthy barley plants for a 2-d inoculation period, and fluorescence of infected plants was evaluated with a hand-held blue green lamp (Luyor Instrument) at 15 dpi. For RNA interference assays, the 600 bp of *LsCK1.3* and the 555 bp of negative control ampicillin resistance gene *β-lactamase* fragments (Amp) containing T7 promoters at the two termini were amplified. Before injection, second-instar nymphs were anesthetized by incubation on ice for 30 min. Next, ~70 ng of ds*LsCK1* and ds*Amp* were mixed with crude virus extracts from Agrobacterium-infiltrated regions of *N. benthamiana* leaves that were exhibiting GFP fluorescence, and 23 nL was injected into the thoraxes of each insect with a Nanoinject II auto-nanoliter injector (Drummond Scientific). RNA interference effects and virus accumulation were detected by RT-qPCR at 5 dpi. All primers are listed in Supplemental Data Set 1.

Trypan Blue Staining

Trypan blue staining was performed as previously reported, with minor modifications, by Zhang et al. (2018). *N. benthamiana* leaves infiltrated with Agrobacterium cultures were soaked in ethanol for 2 to 3 min and then transferred to staining buffer (10 mL of lactic acid, 10 mL of water phenol, 10 mL of glycerol, and 10 mL of double distilled water with 15 mg of trypan blue), boiled in water for 10 to 15 min, and left to stand for 6 to 8 h at room temperature. Leaves were photographed after destaining three times using chloral hydrate (2.5 g/mL).

Accession Numbers

Sequence data of proteins and genes used this article can be found in Supplemental Data Set 3 and at UniProt protein resource (https://www.uniprot.org/), GenBank database (https://ncbi.nlm.nih.gov), *Nicotiana benthamiana* Genome & Transcriptome database (http://benthgenome.qut.edu.au/), and *Saccharomyces* genome database (https://www.yeastgenome.org/).

Supplemental Data

Supplemental Figure 1. LC-MS/MS analysis of the SR motif phosphorylation of BYSMV P.

Supplemental Figure 2. RFP accumulation from agMR after coexpression with SR motif P protein mutants deficient in phosphorylation.

Supplemental Figure 3. Immunoblot analysis showing accumulation of P and M in co-infiltrated *N. benthamiana* leaves at 10 dpi.

Supplemental Figure 4. GFP foci in *N. benthamiana* leaves at 10 d post infiltration with Agrobacterium cultures containing the indicated plasmids.

Supplemental Figure 5. BiFC assays showing interaction of P/P mutants with themselves or with the BYSMV N protein.

Supplemental Figure 6. BiFC assays showing the negative controls of Rubisco with P/P mutants and N.

Supplemental Figure 7. The presence of N and genome RNA in the purified N–RNA complexes.

Supplemental Figure 8. Immunoblot analysis showing two phosphorylation forms of the BYSMV P protein in yeast.

Supplemental Figure 9. Phylogenetic analysis of the protein sequences of conserved protein kinases.

Supplemental Figure 10. Yeast HRR25 phosphorylates the SR motif of BYSMV P.

Supplemental Figure 11. Phylogenetic analysis of CK1 orthologs based on their protein sequences.

Supplemental Figure 12. Orthologs of yeast HRR25 phosphorylates the SR motif of BYSMV P.

Supplemental Figure 13. BiFC assays showing the negative controls of Rubisco with P and NbCK1.3.

Supplemental Figure 14. Overexpression of CK1, but not a dominant-negative mutant, results in cell death.

Supplemental Figure 15. Overexpression of *Nb*CK1.13 suppresses BYSMV infections in *N. benthamiana* plants.

Supplemental Figure 16. Overexpression of a CK1 dominant-negative mutant suppresses BYSMV infections in plants.

Supplemental Figure 17. Transcript levels of *CK1* genes in response to BYSMV infections in barley plants.

Supplemental Figure 18. Potential phosphorylation sites within the predicted C- terminal IDRs of P proteins.

Supplemental Table. BYSMV P phosphopeptides identified by mass.

Supplemental Data Set 1. Primers used in this study.

Supplemental Data Set 2. Statistical analysis data in this study.

Supplemental Data Set 3. Accession numbers for all CK1 proteins described in this study.

Supplemental File 1. Alignment of conserved kinases in yeast, barley and planthopper.

Supplemental File 2. The phylogenetic tree of yeast, barley and planthopper conserved kinases (Newick format).

Supplemental File 3. Alignments of *Nb*CK1, *Ls*CK1, and *Hv*CK1 orthologs.

Supplemental File 4. The phylogenetic tree of *Nb*CK1, *Ls*CK1, and *Hv*CK1 orthologs (Newick format).

Supplemental Movie 1. Intracellular movement of the BiFC punctate particles of Y^N-P and Y^C-*Nb*CK1.3.

Supplemental Movie 2. Intracellular movement of the BiFC punctate particles of Y^C-P and Y^N-*Nb*CK1.3.

Supplemental Movie 3. A representative movie showing trafficking granules formed by L-mCherry and CFP-N with Y^N-P/Y^C-*Nb*CK1.3.

Supplemental Movie 4. A representative movie showing trafficking granules formed by L-mCherry and CFP-N with Y^C-P/Y^N-*Nb*CK1.3.

ACKNOWLEDGMENTS

We thank our colleagues Chenggui Han, Dawei Li, and Yongliang Zhang for their helpful suggestions and constructive criticism. We thank our colleague Qun He for his gift of the GST antibody. We thank Andrew O. Jackson (Department of Plant and Microbial Biology, University of California, Berkeley) for his gift of pGD and pGDG and for helpful suggestions. We thank Xiaorong Tao (Department of Plant Pathology, Nanjing Agricultural University) for his gift of the pCB301-2×35S-Nos plasmid. We thank Zhen Li for his assistance with LC-MS/MS analysis at the Mass Spectrometry Facility of China Agricultural University. This work was supported by the National Natural Science Foundation of China (grants 31872920 and 31571978).

AUTHOR CONTRIBUTIONS

X.-B.W., Q.G., T.Y., and Z.-J.Z. conceived and designed the experiments; Q.G., T.Y., X.-D.F., Z.-J.Z., Z.-H.D., Q.C., W.-Y.X., D.-M.G., J.-H.Q., and Y.-Z.Y. performed the experiments; X.-B.W., Q.G., T.Y., and S.-Y.L. analyzed the data and drafted the article; X.-B.W., Y.W., and J.Y. participated in experimental coordination and revision of the article; and X.-B.W., Q.G., and T.Y. proofread and finalized the article.

Received May 11, 2020; revised June 24, 2020; accepted July 7, 2020; published July 8, 2020.

REFERENCES

Ammar, D., Tsai, C.-W., Whitfield, A.E., Redinbaugh, M.G., and Hogenhout, S.A. (2009). Cellular and molecular aspects of rhabdovirus interactions with insect and plant hosts. Annu. Rev. Entomol. **54:** 447–468.

Barik, S., and Banerjee, A.K. (1992). Sequential phosphorylation of the phosphoprotein of vesicular stomatitis virus by cellular and viral protein kinases is essential for transcription activation. J. Virol. **66:** 1109–1118.

Bond, A.E., Row, P.E., and Dudley, E. (2011). Post-translation modification of proteins; methodologies and applications in plant sciences. Phytochemistry **72:** 975–996.

Cao, Q., Xu, W.-Y., Gao, Q., Jiang, Z.-H., Liu, S.-Y., Fang, X.-D., Gao, D.-M., Wang, Y., and Wang, X.-B. (2018). Transmission characteristics of barley yellow striate mosaic virus in its planthopper vector *Laodelphax striatellus*. Front. Microbiol. **9:** 1419.

Chen, L., Zhang, S., Banerjee, A.K., and Chen, M. (2013). N-Terminal phosphorylation of phosphoprotein of *vesicular stomatitis virus* is required for preventing nucleoprotein from binding to cellular RNAs and for functional template formation. J. Virol. **87:** 3177–3186.

Chen, M., Ogino, T., and Banerjee, A.K. (2007). Interaction of vesicular stomatitis virus P and N proteins: identification of two overlapping domains at the N terminus of P that are involved in N0-P complex formation and encapsidation of viral genome RNA. J. Virol. **81:** 13478–13485.

Cheng, J.L., Sweredoski, M.J., and Baldi, P. (2005). Accurate prediction of protein disordered regions by mining protein structure data. Data Min. Knowl. Discov. **11:** 213–222.

Dietzgen, R.G., Bejerman, N.E., Goodin, M.M., Higgins, C.M., Huot, O.B., Kondo, H., Martin, K.M., and Whitfield, A.E. (2020). Diversity and epidemiology of plant rhabdoviruses. Virus Res. **281:** 197942.

Dong, K., Wang, Y., Zhang, Z., Chai, L.X., Tong, X., Xu, J., Li, D., and Wang, X.B. (2016). Two amino acids near the N-terminus of Cucumber mosaic virus 2b play critical roles in the suppression of RNA silencing and viral infectivity. Mol. Plant Pathol. **17:** 173–183.

Dosztányi, Z., Csizmok, V., Tompa, P., and Simon, I. (2005). IUPred: Web server for the prediction of intrinsically unstructured regions of proteins based on estimated energy content. Bioinformatics **21:** 3433–3434.

Emerson, S.U., and Schubert, M. (1987). Location of the binding domains for the RNA polymerase L and the ribonucleocapsid template within different halves of the NS phosphoprotein of vesicular stomatitis virus. Proc. Natl. Acad. Sci. USA **84:** 5655–5659.

Emerson, S.U., and Yu, Y. (1975). Both NS and L proteins are required for in vitro RNA synthesis by vesicular stomatitis virus. J. Virol. **15:** 1348–1356.

Fang, X.D., Yan, T., Gao, Q., Cao, Q., Gao, D.M., Xu, W.Y., Zhang, Z.J., Ding, Z.H., and Wang, X.B. (2019). A cytorhabdovirus phosphoprotein forms mobile inclusions trafficked on the actin/ER network for viral RNA synthesis. J. Exp. Bot. **70:** 4049–4062.

Friso, G., and van Wijk, K.J. (2015). Posttranslational protein modifications in plant metabolism. Plant Physiol. **169:** 1469–1487.

Gao, Q., Xu, W.-Y., Yan, T., Fang, X.-D., Cao, Q., Zhang, Z.-J., Ding, Z.-H., Wang, Y., and Wang, X.-B. (2019). Rescue of a plant cytorhabdovirus as versatile expression platforms for planthopper and cereal genomic studies. New Phytol. **223:** 2120–2133.

Gerard, F.C., Ribeiro, Ede.A., Jr., Leyrat, C., Ivanov, I., Blondel, D., Longhi, S., Ruigrok, R.W., and Jamin, M. (2009). Modular organization of rabies virus phosphoprotein. J. Mol. Biol. **388:** 978–996.

Green, T.J., and Luo, M. (2009). Structure of the vesicular stomatitis virus nucleocapsid in complex with the nucleocapsid-binding domain of the small polymerase cofactor, P. Proc. Natl. Acad. Sci. USA **106:** 11713–11718.

Gross, S.D., and Anderson, R.A. (1998). Casein kinase I: Spatial organization and positioning of a multifunctional protein kinase family. Cell. Signal. **10:** 699–711.

Gupta, A.K., Blondel, D., Choudhary, S., and Banerjee, A.K. (2000). The phosphoprotein of rabies virus is phosphorylated by a unique cellular protein kinase and specific isomers of protein kinase C. J. Virol. **74:** 91–98.

He, Z., Zhang, H., Gao, S., Lercher, M.J., Chen, W.H., and Hu, S. (2016). Evolview v2: An online visualization and management tool for customized and annotated phylogenetic trees. Nucleic Acids Res. **44:** W236–W241.

Heger-Stevic, J., Zimmermann, P., Lecoq, L., Böttcher, B., and Nassal, M. (2018). Hepatitis B virus core protein phosphorylation: Identification of the SRPK1 target sites and impact of their occupancy on RNA binding and capsid structure. PLoS Pathog. **14:** e1007488.

Hirose, S., Shimizu, K., Kanai, S., Kuroda, Y., and Noguchi, T. (2007). POODLE-L: A two-level SVM prediction system for reliably predicting long disordered regions. Bioinformatics **23:** 2046–2053.

Hoover, H.S., and Kao, C.C. (2016). Phosphorylation of the viral coat protein regulates RNA virus infection. Virus Adapt. Treat. **8:** 13–20.

Hu, Y., Li, Z., Yuan, C., Jin, X., Yan, L., Zhao, X., Zhang, Y., Jackson, A.O., Wang, X., Han, C., Yu, J., and Li, D. (2015). Phosphorylation of TGB1 by protein kinase CK2 promotes barley stripe mosaic virus movement in monocots and dicots. J. Exp. Bot. **66:** 4733–4747.

Hwang, L.N., Englund, N., Das, T., Banerjee, A.K., and Pattnaik, A.K. (1999). Optimal replication activity of vesicular stomatitis virus RNA polymerase requires phosphorylation of a residue(s) at carboxy-terminal domain II of its accessory subunit, phosphoprotein P. J. Virol. **73:** 5613–5620.

Ishida, T., and Kinoshita, K. (2007). PrDOS: Prediction of disordered protein regions from amino acid sequence. Nucleic Acids Res. **35:** W460–W464.

Ivanov, I., Yabukarski, F., Ruigrok, R.W.H., and Jamin, M. (2011). Structural insights into the rhabdovirus transcription/replication complex. Virus Res. **162:** 126–137.

Jackson, A.O., Dietzgen, R.G., Goodin, M.M., Bragg, J.N., and Deng, M. (2005). Biology of plant rhabdoviruses. Annu. Rev. Phytopathol. **43:** 623–660.

Jackson, A.O., and Li, Z. (2016). Developments in plant negative-strand RNA virus reverse genetics. Annu. Rev. Phytopathol. **54:** 469–498.

Jakubiec, A., and Jupin, I. (2007). Regulation of positive-strand RNA virus replication: The emerging role of phosphorylation. Virus Res. **129:** 73–79.

Knippschild, U., Gocht, A., Wolff, S., Huber, N., Löhler, J., and Stöter, M. (2005). The casein kinase 1 family: Participation in multiple cellular processes in eukaryotes. Cell. Signal. **17:** 675–689.

Kumar, S., Stecher, G., and Tamura, K. (2016). MEGA7: Molecular evolutionary genetics analysis version 7.0 for bigger datasets. Mol. Biol. Evol. **33:** 1870–1874.

Lee, H., Chen, R., Lee, Y., Yoo, S., and Lee, C. (2009). Essential roles of CKIdelta and CKIepsilon in the mammalian circadian clock. Proc. Natl. Acad. Sci. USA **106:** 21359–21364.

Lee, J.Y., Taoka, K., Yoo, B.C., Ben-Nissan, G., Kim, D.J., and Lucas, W.J. (2005). Plasmodesmal-associated protein kinase in tobacco and Arabidopsis recognizes a subset of non-cell-autonomous proteins. Plant Cell **17:** 2817–2831.

Leyrat, C., Ribeiro, E.A., Gerard, F.C.A., Ivanov, I., Ruigrok, R.W.H., and Jamin, M. (2011). Structure, interactions with host cell and functions of rhabdovirus phosphoprotein. Future Virol. **6:** 465–481.

Li, L., Stoeckert, C.J., Jr., and Roos, D.S. (2003). OrthoMCL: Identification of ortholog groups for eukaryotic genomes. Genome Res. **13:** 2178–2189.

Linding, R., Jensen, L.J., Diella, F., Bork, P., Gibson, T.J., and Russell, R.B. (2003). Protein disorder prediction: Implications for structural proteomics. Structure **11:** 1453–1459.

Liu, W., Xu, Z.-H., Luo, D., and Xue, H.-W. (2003). Roles of OsCKI1, a rice casein kinase I, in root development and plant hormone sensitivity. Plant J. **36:** 189–202.

Mann, K.S., and Dietzgen, R.G. (2014). Plant rhabdoviruses: New insights and research needs in the interplay of negative-strand RNA viruses with plant and insect hosts. Arch. Virol. **159:** 1889–1900.

Mei, Y., Wang, Y., Hu, T., Yang, X., Lozano-Duran, R., Sunter, G., and Zhou, X. (2018). Nucleocytoplasmic shuttling of Geminivirus C4 protein mediated by phosphorylation and myristoylation is critical for viral pathogenicity. Mol. Plant **11:** 1466–1481.

Millar, A.H., Heazlewood, J.L., Giglione, C., Holdsworth, M.J., Bachmair, A., and Schulze, W.X. (2019). The scope, functions, and dynamics of posttranslational protein modifications. Annu. Rev. Plant Biol. **70:** 119–151.

Mondal, A., Victor, K.G., Pudupakam, R.S., Lyons, C.E., and Wertz, G.W. (2014). Newly identified phosphorylation site in the vesicular stomatitis virus P protein is required for viral RNA synthesis. J. Virol. **88:** 1461–1472.

Moyer, S.A., Smallwood-Kentro, S., Haddad, A., and Prevec, L. (1991). Assembly and transcription of synthetic vesicular stomatitis virus nucleocapsids. J. Virol. **65:** 2170–2178.

Obradovic, Z., Peng, K., Vucetic, S., Radivojac, P., and Dunker, A.K. (2005). Exploiting heterogeneous sequence properties improves prediction of protein disorder. Proteins **61:** 176–182.

Pattnaik, A.K., Hwang, L., Li, T., Englund, N., Mathur, M., Das, T., and Banerjee, A.K. (1997). Phosphorylation within the amino-terminal acidic domain I of the phosphoprotein of vesicular stomatitis virus is required for transcription but not for replication. J. Virol. **71:** 8167–8175.

Peck, S.C. (2006). Analysis of protein phosphorylation: Methods and strategies for studying kinases and substrates. Plant J. **45:** 512–522.

Qanungo, K.R., Shaji, D., Mathur, M., and Banerjee, A.K.J.P.N.A.S. (2004). Two RNA polymerase complexes from vesicular stomatitis virus-infected cells that carry out transcription and replication of genome RNA. Proc. Natl. Acad. Sci. USA **101:** 5952–5957.

Rahmeh, A.A., Morin, B., Schenk, A.D., Liang, B., Heinrich, B.S., Brusic, V., Walz, T., and Whelan, S.P.J. (2012). Critical phosphoprotein elements that regulate polymerase architecture and function in vesicular stomatitis virus. Proc. Natl. Acad. Sci. USA **109:** 14628–14633.

Rena, G., Bain, J., Elliott, M., and Cohen, P. (2004). D4476, a cell-permeant inhibitor of CK1, suppresses the site-specific phosphorylation and nuclear exclusion of FOXO1a. EMBO Rep. **5:** 60–65.

Shimizu, K., Hirose, S., and Noguchi, T. (2007). POODLE-S: Web application for predicting protein disorder by using physicochemical features and reduced amino acid set of a position-specific scoring matrix. Bioinformatics **23:** 2337–2338.

Spolar, R.S., and Record, M.T., Jr. (1994). Coupling of local folding to site-specific binding of proteins to DNA. Science **263:** 777–784.

Takamatsu, F., Asakawa, N., Morimoto, K., Takeuchi, K., Eriguchi, Y., Toriumi, H., and Kawai, A. (1998). Studies on the rabies virus RNA polymerase: 2. Possible relationships between the two forms of the non-catalytic subunit (P protein). Microbiol. Immunol. **42:** 761–771.

Tan, S.T., Dai, C., Liu, H.-T., and Xue, H.-W. (2013). Arabidopsis casein kinase1 proteins CK1.3 and CK1.4 phosphorylate cryptochrome2 to regulate blue light signaling. Plant Cell **25:** 2618–2632.

Tan, S.T., and Xue, H.W. (2014). Casein kinase 1 regulates ethylene synthesis by phosphorylating and promoting the turnover of ACS5. Cell Rep. **9:** 1692–1702.

Tuffereau, C., Fischer, S., and Flamand, A. (1985). Phosphorylation of the N and M1 proteins of rabies virus. J. Gen. Virol. **66:** 2285–2289.

Uversky, V.N., Oldfield, C.J., and Dunker, A.K. (2005). Showing your ID: Intrinsic disorder as an ID for recognition, regulation and cell signaling. J. Mol. Recognit. **18:** 343–384.

Vullo, A., Bortolami, O., Pollastri, G., and Tosatto, S.C.E. (2006). Spritz: A server for the prediction of intrinsically disordered regions in protein sequences using kernel machines. Nucleic Acids Res. **34:** W164–W168.

Walker, P.J., Dietzgen, R.G., Joubert, D.A., and Blasdell, K.R. (2011). Rhabdovirus accessory genes. Virus Res. **162:** 110–125.

Wang, A. (2015). Dissecting the molecular network of virus-plant interactions: The complex roles of host factors. Annu. Rev. Phytopathol. **53:** 45–66.

Wang, Q., Ma, X., Qian, S., Zhou, X., Sun, K., Chen, X., Zhou, X., Jackson, A.O., and Li, Z. (2015). Rescue of a plant negative-strand RNA virus from cloned cDNA: Insights into enveloped plant virus movement and morphogenesis. PLoS Pathog. **11:** e1005223.

Wright, P.E., and Dyson, H.J. (2009). Linking folding and binding. Curr. Opin. Struct. Biol. **19:** 31–38.

Yan, T., Zhu, J.R., Di, D., Gao, Q., Zhang, Y., Zhang, A., Yan, C., Miao, H., and Wang, X.B. (2015). Characterization of the complete genome of Barley yellow striate mosaic virus reveals a nested gene encoding a small hydrophobic protein. Virology **478:** 112–122.

Yang, M., Zhang, Y., Xie, X., Yue, N., Li, J., Wang, X.B., Han, C., Yu, J., Liu, Y., and Li, D. (2018). *Barley stripe mosaic virus* γb protein subverts autophagy to promote viral infection by disrupting the ATG7-ATG8 Interaction. Plant Cell **30:** 1582–1595.

Yang, Z.R., Thomson, R., McNeil, P., and Esnouf, R.M. (2005). RONN: The bio-basis function neural network technique applied to the detection of natively disordered regions in proteins. Bioinformatics **21:** 3369–3376.

Zhang, K., Zhang, Y., Yang, M., Liu, S., Li, Z., Wang, X., Han, C., Yu, J., and Li, D. (2017a). The Barley stripe mosaic virus γb protein promotes chloroplast-targeted replication by enhancing unwinding of RNA duplexes. PLoS Pathog. **13:** e1006319.

Zhang, S., Chen, L., Zhang, G., Yan, Q., Yang, X., Ding, B., Tang, Q., Sun, S., Hu, Z., and Chen, M. (2013). An amino acid of human parainfluenza virus type 3 nucleoprotein is critical for template function and cytoplasmic inclusion body formation. J. Virol. **87:** 12457–12470.

Zhang, T., Faraggi, E., Xue, B., Dunker, A.K., Uversky, V.N., and Zhou, Y. (2012). SPINE-D: Accurate prediction of short and long disordered regions by a single neural-network based method. J. Biomol. Struct. Dyn. **29:** 799–813.

Zhang, X., Dong, K., Xu, K., Zhang, K., Jin, X., Yang, M., Zhang, Y., Wang, X., Han, C., Yu, J., and Li, D. (2018). Barley stripe mosaic virus infection requires PKA-mediated phosphorylation of γb for suppression of both RNA silencing and the host cell death response. New Phytol. **218:** 1570–1585.

Zhang, X.-P., Liu, D.-S., Yan, T., Fang, X.-D., Dong, K., Xu, J., Wang, Y., Yu, J.-L., and Wang, X.-B. (2017b). Cucumber mosaic virus coat protein modulates the accumulation of 2b protein and antiviral silencing that causes symptom recovery in planta. PLoS Pathog. **13:** e1006522.

Zhang, Z.-J., et al. (2020). CCR4, a RNA decay factor, is hijacked by a plant cytorhabdovirus phosphoprotein to facilitate virus replication. eLife **9:** e53753.

Zhao, X., Wang, X., Dong, K., Zhang, Y., Hu, Y., Zhang, X., Chen, Y., Wang, X., Han, C., Yu, J., and Li, D. (2015). Phosphorylation of Beet black scorch virus coat protein by PKA is required for assembly and stability of virus particles. Sci. Rep. **5:** 11585.

Zhong, X., Wang, Z.Q., Xiao, R., Cao, L., Wang, Y., Xie, Y., and Zhou, X. (2017). Mimic phosphorylation of a βC1 protein encoded by TYLCCNB impairs its functions as a viral suppressor of RNA silencing and a symptom determinant. J. Virol. **91:** e00300–e00317.

Zhu, J., Shibasaki, F., Price, R., Guillemot, J.-C., Yano, T., Dötsch, V., Wagner, G., Ferrara, P., and McKeon, F. (1998). Intramolecular masking of nuclear import signal on NF-AT4 by casein kinase I and MEKK1. Cell **93:** 851–861.

Zuo, J., Niu, Q.-W., and Chua, N.-H. (2000). Technical advance: An estrogen receptor-based transactivator XVE mediates highly inducible gene expression in transgenic plants. Plant J. **24:** 265–273.